3-2002

Extratropical Transition of Southwest Pacific Tropical Cyclones. Part I: Climatology and Mean Structure Changes

Mark R. Sinclair
Embry-Riddle Aeronautical University, sinclam@erau.edu

Scholarly Commons Citation

Sinclair, M. R. (2002). Extratropical Transition of Southwest Pacific Tropical Cyclones. Part I: Climatology and Mean Structure Changes. *Monthly Weather Review, 130*(3). https://doi.org/10.1175/1520-0493(2002)130<0590:ETOSPT>2.0.CO;2

Extratropical Transition of Southwest Pacific Tropical Cyclones. Part I: Climatology and Mean Structure Changes

MARK R. SINCLAIR

Embry-Riddle Aeronautical University, Prescott, Arizona

(Manuscript received 12 October 2000, in final form 4 September 2001)

ABSTRACT

A database of tropical cyclone best track and intensity information for the southwest Pacific Ocean basin is used to construct a 28-year climatology for tropical cyclones that move into middle latitudes. Of the nine or so tropical cyclones that form each year, an average of about three can be expected to migrate south of 35°S, with the greatest fraction in March. Storms entering the Tasman Sea west of New Zealand (NZ) move almost due south on average and retain greater intensity than those to the east of NZ, where storms decay quickly while moving rapidly away to the southeast. Storms east of NZ are embedded in a stronger, more zonal flow than those to the west, which move poleward ahead of a larger-amplitude trough. During El Niño years, tropical cyclones that move into middle latitudes exhibit stronger zonal motion and occur over a wider range of longitudes than during La Niña years. Storm intensity is only weakly correlated with concurrent SST anomalies, suggesting that atmospheric circulation is the dominant influence on storm properties.

Average structure changes during extratropical transition (ET) are identified using the NCEP–NCAR reanalysis dataset, for a subset of 33 transitioning storms during 1980–97. Composites are used to construct a three-dimensional conceptual model of the transformation from a mature hurricane to an asymmetric baroclinic midlatitude cyclone. Southwest Pacific tropical cyclones encounter the baroclinic westerlies early in their lives, accounting for their average eastward (and poleward) motion. At maximum average intensity near 20°S, baroclinic effects are already important, with warm frontogenesis appearing in the southeast quadrant and outflow aloft into a downstream subtropical wind maximum that moves poleward with the storm. By 25°S, the average TC has lost the characteristic symmetric anticyclonic outflow aloft and acquired the characteristics of a baroclinic midlatitude storm, including regions of warm and cold frontogenesis, a vertical motion dipole and a westward tilt with height. From about 30°S poleward, a second upper-tropospheric wind maximum appears west of the storm, with strengthening cyclonic vorticity advection aloft. Below about 400 hPa, the storm retains the vertical, warm cyclonic core as it migrates poleward.

1. Introduction

Extratropical transition (ET) occurs when a tropical storm moves into middle latitudes and progressively acquires characteristics of a baroclinic midlatitude system. As the tropical cyclone (TC) moves poleward, it loses its tropical characteristics when it moves over cooler water and encounters the increasing vertical wind shears associated with the midlatitude westerlies. During this time, it typically loses its distinctive symmetric upper-level circulation and cloud shield, which commonly shears off poleward and eastward. Eventually, increasing thermal advection brings cooler and drier air into the western sector of the storm, which progressively acquires the asymmetric cloud and thermal characteristics of a midlatitude frontal cyclone. These structure changes associated with the poleward movement of a TC are termed extratropical transformation.

As TCs move into middle latitudes, they often maintain sufficient vigor to produce damaging winds, high seas, and heavy rain in middle latitudes. Occasionally, TC remnants reintensify in the extratropics to become potent midlatitude storms capable of inflicting loss of life and severe property damage. Several memorable ET events have occurred in the southwest Pacific Ocean basin. In April 1968, TC Gisele reintensified as it moved south over New Zealand (NZ), producing winds gusting to 75 m s^{-1} in the capital city of Wellington, and sinking the interisland ferry *Wahine* with the loss of 51 lives (Hill 1970). Cyclone Bola dumped over 900 mm of rain and produced hurricane-force winds in regions of northern NZ in March 1988 (Sinclair 1993b). A colorful description of the ''Cyclone of '36'' (an ET event), probably the most damaging storm of the twentieth century to hit NZ, is found in Brenstrum (1997). Notable examples from the Northern Hemisphere (NH) include the regeneration of Hurricane Hazel as a powerful extra-

Corresponding author address: Dr. Mark R. Sinclair, Embry-Riddle Aeronautical University, 3800 Willow Creek Road, Prescott, AZ 86301.
E-mail: sinclam@pr.erau.edu

tropical storm over Canada (Palmén 1958) and Hurricane Agnes which produced one of the worst natural flooding disasters in United States history over the northeast of the country (Carr and Bosart 1978; DiMego and Bosart 1982a,b; Bosart and Dean 1991). While maximum winds in these transformed storms may be weaker than in the parent hurricane, the areas of damaging wind, high seas, and heavy rain are typically much larger (Hart and Evans 2001), increasing the potential for loss of life and property damage.

In comparison with the effort devoted to the respective study of tropical and extratropical cyclones, the transformation from TC to extratropical cyclone is only now starting to receive attention. Research agendas have been typically restricted to either tropical or midlatitude storms, with hybrid transition cases often falling between the cracks. For example, there has never been a major field campaign devoted to ET. This lack of attention is surprising considering the loss of life and billions of dollars of damage caused by past ET events, and the fact that they continue to be rather poorly forecast (Browning et al. 1998; Klein et al. 2000). Once the tropical storm ''goes extratropical,'' national hurricane centers typically cease monitoring efforts like aircraft reconnaissance, even though the potential for reintensification remains. Consequently, data on storms that retain or regain damaging winds and/or precipitation in middle latitudes are often incomplete, especially where storms move away from land. This difficulty is compounded by the practice of keeping tropical and extratropical storm databases separate, making it difficult to obtain coherent information on past ET events throughout the life of the storm. Assessment of hazard risk is thus hampered by the dearth of statistical information from past ET events. Clearly, there is a need to separately assemble basic statistics for past extratropical transition events for each of the ocean basins.

At a recent ET Workshop funded by the Risk Prediction Initiative (RPI), a science–business partnership funded by seven (re)insurance companies, delegates advocated a research agenda (Malmquist 1999; also available on the world wide web at www.bbsr.edu/rpi) to address these and other issues. Of relevance to the present work were recommendations to compile basic statistics of ET events in the various ocean basins, to continue research aimed at better characterization of the synoptic and physical processes involved in ET, and to construct a reliable conceptual model for the transforming storm.

Much of this ground-breaking survey work is already under way for several ocean basins. For the western North Pacific, Brand and Guard (1978) and Klein et al. (2000) have completed basic climatologies, Harr et al. (2000) examined a large number of past ET events to identify the impact of midlatitude circulation characteristics on ET evolution, while Harr and Elsberry (2000) examined the evolution of storm structure during the transition process. Hart and Evans (2001) have compiled basic statistics for North Atlantic ET events. For the Southern Hemisphere (SH), Foley and Hanstrum (1994) assembled statistics and composite MSL pressure analyses for TCs affecting the west coast of Australia.

For the southwest Pacific Ocean basin, a number of basic summaries of TC activity have been undertaken (Kerr 1976; Revell 1981; Holland 1983; Thompson et al. 1992; Radford et al. 1996); its relation to the phase of the El Niño–Southern Oscillation (ENSO) cycle has been examined (Nichols 1984; Revell and Goulter 1986a,b; Hastings 1990; Basher and Zheng 1995); and descriptions of individual TCs have been published (Revell 1985, 1986, 1987). However, these studies largely omit any explicit discussion of ET. The decadal summaries of Kerr (1976), Revell (1981) and Thompson et al. (1992) analyze the tracks and intensities of all TCs between 1949 and 1989, including the extratropical phase. Their careful analysis provided much of the raw track and intensity data on which part of the present study is based (see section 2). More detailed synoptic and diagnostic analysis of individual ET events that have impacted NZ includes the studies of Hill (1970), Tomlinson (1975), Trenberth (1977), Littlejohn (1984), and Sinclair (1993a,b). While these case studies have revealed specific insights about particular storms, there remains a need for more systematic study of a larger number of past ET events, as advocated by the RPI Workshop participants.

A preliminary climatology of TCs entering middle latitudes in the southwest Pacific was prepared in an unpublished 1995 report to the Meteorological Service of New Zealand (C. Revell 1996, personal communication), using data from 196 cases of ET during 1969–89. This provided basic statistics of ET and extratropical regeneration and described environmental features that influence TC behavior. Revell found that about half of all TCs decay north of 25°S, with penetration further south most frequent in March toward the end of the season. Of these, extratropical regeneration was favored in March and April (26% and 29% respectively). Most cases of regeneration occur downstream from an amplifying trough in the westerlies over the northern Tasman sea and northern NZ, with markedly fewer cases east of NZ.

The present study consolidates this work by first compiling basic occurrence statistics for 81 TCs that enter middle latitudes in the southwest Pacific. Composites are then used to construct a three-dimensional conceptual model of the transformation from a mature hurricane to an asymmetric baroclinic midlatitude cyclone as the composite storm moves south. A second separate companion paper will examine the variability among composites using a larger database of storms. This second paper will identify the impact of different midlatitude circulation characteristics on ET structure and evolution (e.g., Harr et al. 2000) and will also compare regenerating storms with dissipating ones. The present work provides the first published overview of the cli-

TABLE 1. Classification of southwest Pacific tropical cyclones.

Intensity class	Description	Speed range (kt)	Central pressure (hPa)
1	Tropical depression	<34	>995
2	Gale	34–47	995–986
3	Storm	48–63	985–975
4	Hurricane	>63	<975

matological behavior of ET for the southwest Pacific basin and identifies for the first time, the average structure changes accompanying ET and their relation to the unique climatology of the region.

Following a description of available data (section 2), basic occurrence statistics are presented using archived best track and intensity information (section 3). The gridded reanalysis datasets from the National Centers for Environmental Prediction (NCEP) are then used to describe the typical structure changes during ET and to construct a conceptual model for extratropical transformation (section 4). Section 5 comprises a summary and concluding remarks.

2. Data

a. Track data

Tropical cyclone best track and intensity data for the southwest Pacific basin are based on an archive developed by the New Zealand Meteorological Service (NZMS), henceforth referred to as the NZMS archive. The database compiles time, location, and estimated intensity, plus text comments, for all detected storms since 1939. Entries are based on careful manual reanalysis of all information, including information from hurricane warning centers. Intensity is defined from the maximum sustained wind speed and central pressure in four categories (Table 1), and is aided by interpretation of all available data, including satellite imagery (Dvorak 1975, 1984). In view of the sparse observational network (Fig. 1), in situ measurements of minimum central pressure or maximum core wind speed are rare, so intensity estimates are largely determined by subjective interpretation of satellite imagery. Decadal summaries of TC activity based on information in this database are found in Kerr (1976), Revell (1981), and Thompson et al. (1992), while a more comprehensive analysis has been compiled by Radford et al. (1996). Since about 1969, satellite information has ensured detection and better depiction of all tropical storms. Storms are tracked until their demise, including any extratropical phase. Where ET occurs, the time of extratropical transformation to an extratropical cyclone is not consistently documented as in other ocean basins (e.g., Klein et al. 2000). Where it is documented, it is usually based on subjective interpretation of satellite imagery.

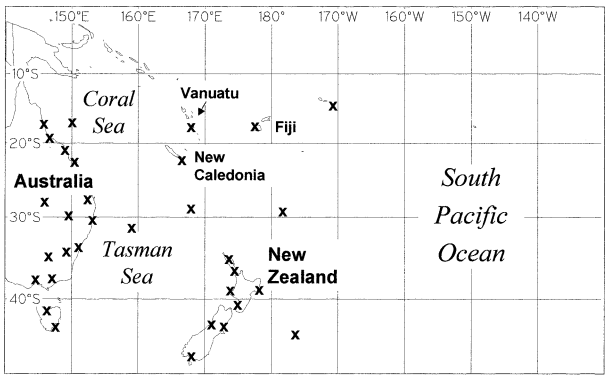

FIG. 1. Map of the southwest Pacific region showing locations of upper-air stations.

b. Gridded analyses

For synoptic and diagnostic analysis, track data are supplemented by gridded numerical analyses. These comprise twice-daily analyses of geopotential height, wind, temperature, relative humidity, and vertical *P*-velocity from the NCEP–National Center for Atmospheric Research (NCAR) reanalysis dataset (Kalnay et al. 1996). These are on a 2.5° × 2.5° latitude–longitude grid. The study region lies downwind from several rawinsonde and surface synoptic observation (SYNOP) stations near Australia and NZ (Fig. 1), with additional island stations north of 30°S. However, the large region south of 25°S and east of 175°W is totally void of any land-based surface or upper-air observations. Ship, aircraft, drifting buoys and remotely sensed measurements help to fill this void, although major shipping and aircraft routes are mostly farther north or in the Tasman Sea. Despite a scarcity of data, Sinclair and Cong (1992) noted that similar numerically analyzed vorticity and ascent fields matched satellite observed cloud and circulation features to within the resolution of the analyses for SH regions thousands of miles from land. This apparent realism, at least on the synoptic scale, justifies continued regular use of similar numerical products at SH forecast offices.

Clearly, data coverage and analysis resolution are inadequate to depict a hurricane's tight inner core, which is typically contained within a 200-km radius. Contour plots prepared from the NCEP analyses revealed many intensity 4 hurricanes with P_{min} analyzed over 1005 hPa (cf. Table 1). Table 2 shows the correlation in several

TABLE 2. Correlation of storm intensity (I) with minimum central pressure (P_{min}) and minimum vorticity (ζ_{min}).

Latitude range	I vs P_{min}	I vs ζ_{min}	No. of points
0°–15°S	−0.48	−0.32	103
15°–20°S	−0.51	−0.55	177
20°–30°S	−0.49	−0.46	183
30°–90°S	−0.39	−0.60	190

latitude bands between storm intensity from the NZMS database (I) and that as estimated from the NCEP analyses by two methods: minimum central pressure (P_{min}) and minimum 1000 hPa vorticity (ζ_{min}). Both P_{min} and ζ_{min} variations are only weakly correlated with I north of 30°S, confirming the shortcomings of estimating hurricane intensity solely from coarse-resolution NCEP analyses. Of course, the correlations in Table 2 are also degraded by uncertainty in the estimates of I. South of 30°S, the correlation of I with ζ_{min} improves, presumably in response to the areal expansion of the low-level circulation that occurs during ET (Muramatsu 1985; Hart and Evans 2001). However, the correlation with P_{min} weakens in middle latitudes, perhaps because changes in storm circulation are not the sole cause of central pressure change. Sinclair (1997) documented how central pressures of SH cyclones can vary without corresponding changes in the circulation about the low. For example, central pressure may change without any corresponding change in circulation strength as a cyclone moves across the strong climatological pressure gradients of the SH midlatitudes.

Despite the limitations of the NCEP data, Sinclair (1993a,b) was able to use a similar 2.5° resolution dataset to describe synoptic-scale influences on the motion, intensity, and precipitation field of TCs Patsy (December 1986) and Bola (March 1988). Although storm core intensity prior to ET was seriously underestimated, there was good correspondence of the location of analyzed circulation and ascent features with satellite imagery as the storms moved into middle latitudes. The present study seeks to document similar synoptic-scale features for a large number of storms that undergo ET. Numerical model products available to NZ forecasters are at a similar resolution, making findings from the present study directly relevant.

3. Climatology of tropical cyclones that move into middle latitudes

In this section, we present some summary statistics for TCs that move into the extratropics of the southwest Pacific as compiled from the NZMS TC archive. The goal is to estimate the number and geographical distribution of TCs that move into middle latitudes, although the limited sample size here deters statistical analysis as comprehensive as that published for NH ocean basins (e.g., Hart and Evans 2001). A secondary objective is to assess how the occurrence of these storms varies in response to well-monitored indices of climate variability like sea surface temperature (SST) and the Southern Oscillation Index (SOI), and identify circulation characteristics associated with poleward-moving storms in different regions. This compilation of basic statistics, although limited by sample size, should assist seasonal forecasts of the likelihood of a TC moving into middle latitudes. Analysis of how tracks vary in relation to different midlatitude circulation characteristics will be addressed in a later companion paper.

In the NZMS archive, no consistent record is made of the nature, timing, or location of structure changes that accompany movement into middle latitudes. The occasional plain language remarks that a TC has gone extratropical are not consistently included and are subjectively based. Thus, we have no record from the NZMS archive which of the storms compiled here have undergone the evolutionary process involving extratropical transformation and possible reintensification that is commonly termed ET. However, as will be seen later in this paper, the baroclinic westerlies extend almost to 15°S in the southwest Pacific. Thus, it would be expected that the majority of TCs that migrate into the extratropics would have also undergone some degree of extratropical transformation.

For the climatological analysis, track data for the 251 southwest Pacific TCs since January 1970 are used. Satellite imagery was first used to locate TCs during 1969 (Revell 1981). Earlier information prior to the advent of satellites is incomplete, with large numbers of storms undetected by the sparse observational network (Fig. 1) prior to 1970. Time series of TC occurrence plotted from the NZMS database (not shown), revealed that the annual average of 5.1 cyclones detected during 1939–69 jumped rather abruptly to around 9.0 after 1970.

a. Overview of southwest Pacific tropical cyclone climatology

To set the scene for this study, we first present some brief summary statistics for the population of all southwest Pacific TCs between 1970 and 1996. Figure 2a shows that the southwest Pacific cyclone season is November through May, with the greatest incidence in February. Instances where TCs make it into midlatitudes, here defined as south of 35°S (Fig. 2b), generally follow the overall occurrence in Fig. 2a. Close to one-third of all TCs (81 out of 251) fall into this category, with the highest fraction in March, in agreement with the unpublished study of Revell cited earlier.

Figure 3 illustrates the geographical distribution of storm properties, based on the full population of 251 TCs since 1970. Figure 3a shows that the area of the Coral Sea just north of New Caledonia (see Fig. 1 for location of places referred to in text) is home to the greatest number of TCs. Contour values are the numbers of TC centers passing within 555 km (5° of latitude) of a given point per year, where each storm is counted just once at each point. Looking at the southern extremities of the distribution in Fig. 3a, poleward-moving TCs are most commonly found over the waters west and east of NZ, with a very slight tendency for storms to avoid NZ itself. On average, New Zealand's major population center, Auckland (37°S, 175°E), can expect to be under the influence of just over one tropical cyclone per year. Average storm motion (Fig. 3b) is toward the southeast

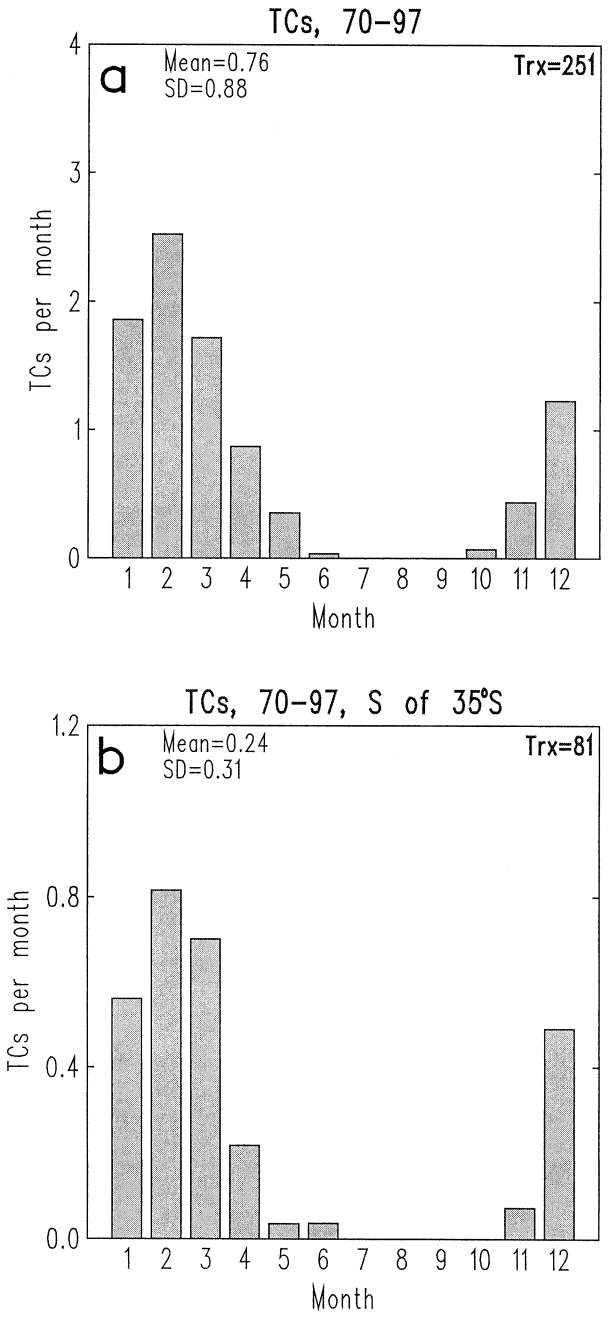

FIG. 2. Frequency by month of (a) all tropical cyclones in the southwest Pacific and (b) just tropical cyclones progressing south of 35°S. The total number of storms is shown in the top right.

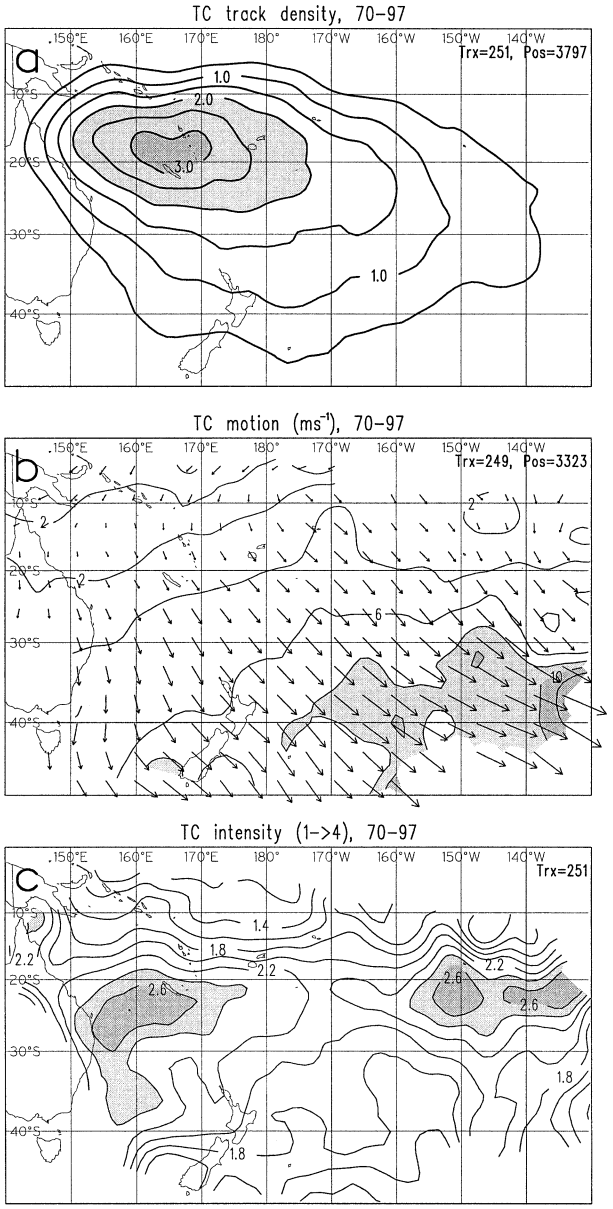

FIG. 3. Average distribution, motion, and intensity for all tropical cyclones during 1970–97. (a) Distribution. Contours representing the number of tropical cyclones passing within 555 km of each point per year, drawn every 0.5, with values >2 and 3 shaded. (b) Average storm motion vectors, with speed contours added, every 2 m s^{-1}, with speeds >8 and 10 m s^{-1} shaded. (c) Average intensity, with values >2.4 and 2.6 intensity units shaded (see Table 1).

over most of the region, with acceleration as they move poleward. Unlike in other ocean basins (Elsberry 1987), most southwest Pacific TCs have an eastward component of motion during most of their life, with many tracking eastward throughout their entire life. Average *westward* motion is found only in a small region west of the dateline and north of about 12°S. Track variability, not addressed in the present paper, is smoothed out by the averaging used here. Kerr (1976) and Revell (1981) identified four basic track types. The reader is referred to these and other publications cited earlier for a more comprehensive analysis of southwest Pacific tropical cyclone motion.

Intensity characteristics are examined in Fig. 3c. Because the NCEP analyses are too coarse to realistically depict the tropical cyclone inner core, the best intensity

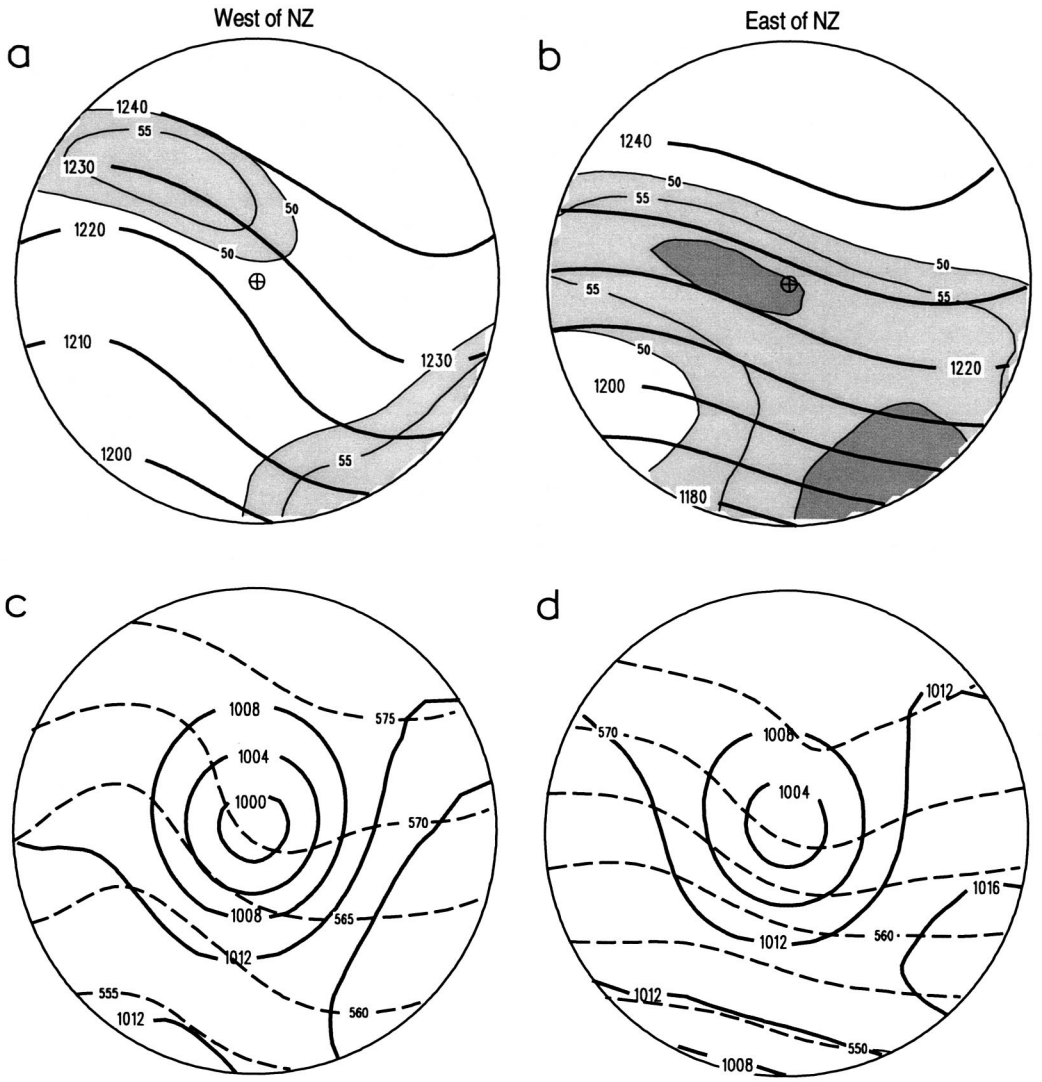

FIG. 4. (a) Composite 200-hPa height, every 10 dam (thick, solid) and isotachs, every 5 kt from 50 kt upwards, with values >50 and 60 kt shaded, for storms west of NZ. (b) As for (a) except for storms east of NZ. (c), (d) As for (a), (b) except MSL pressure, every 4 hPa (solid) and 1000–500-hPa thickness, every 5 dam (dashed).

estimates (Table 1) contained in the NZMS track database are used. Average intensity (Fig. 3c) maximizes in the 20°–25°S latitude band in two regions—one south of New Caledonia and the other east of the dateline, with a lobe of high average intensity extending south into the Tasman Sea. The picture here is of TCs forming and intensifying in the tropics as they slowly move poleward, reaching maximum intensity near 20°–25°S then weakening while accelerating southeast out of the Tropics.

There are differences between storms moving poleward east of NZ and those to the west. On average, storms over the Tasman Sea west of NZ move slowly southward with little acceleration (Fig. 3b) and are about 0.5 intensity units stronger than those to the east (Fig. 3c). The greater intensity west of NZ is possibly due to the warm east Australian current. East of NZ, storms weaken more rapidly and exhibit translations to the southeast rather than to the south, at speeds nearly double those to the west. In addition, storms affect the region west of NZ earlier in the season, occurring with equal frequency during each of the months December through March (not shown, cf. Fig. 2). East of NZ, the frequency of poleward-moving TCs peaks in February and March, with December cases comparatively rare.

The differences between storms east and west of NZ are consistent with differences in the environmental flow. Figure 4 shows composites of upper and lower flow fields at the time in each track closest to 35°S, for 14 storms between 150°E and 160°E (Figs. 4a,c) and 15 storms between 170°E and 170°W (Figs. 4b,d). The storms chosen occurred between 1980 and 1997 and composites are based on NCEP data. Compositing is

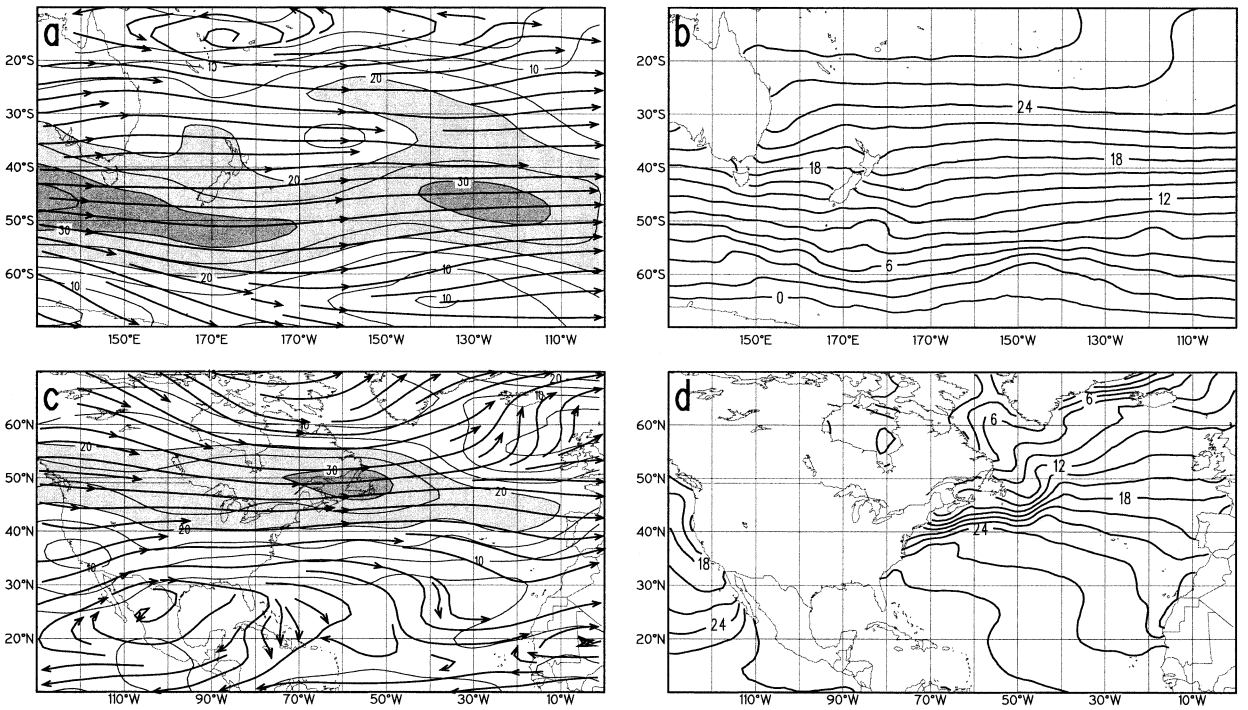

FIG. 5. (a) Average Feb 200-hPa streamlines and isotachs, every 5 m s^{-1}, with values >30 m s^{-1} shaded. (b) Average Feb SST (°C), every 2°C. (c), (d) As for (a), (b) except for North Atlantic, Sep.

performed on a subgrid centered on each storm and uses the methodology described more fully in section 4a. Storms east of NZ are embedded in stronger, more zonal upper-level flow than those to the west, accounting for their faster, more zonal movement. Storms west of NZ feature a stronger sea level circulation, consistent with Fig. 3c and a sharper and more diffluent upstream trough, but slightly weaker baroclinity.

The distinctive behavior of southwest Pacific TCs appears related to climatological and geographical features of the area. During the TC season, the time-averaged upper-level westerlies extend to about 15°S (Fig. 5a). Similar flow patterns are found at other levels above about 600 hPa (not shown), with lighter easterly flow below that level north of 30°S. Consequently, most storms have an eastward component of motion (Fig. 3b) and encounter the equatorward flank of the upper westerlies early in their life. As these TCs track poleward, they encounter steadily decreasing SSTs (Fig. 5b) that fall below 26°C south of 25°S. Because transitioning South Pacific TCs encounter the midlatitude westerlies and cooler water at rather low latitudes, only 4 out of the 113 storms that have attained hurricane intensity since 1970 have maintained hurricane strength poleward of 30°S.

In contrast, it is not at all unusual for storms in the North Atlantic and northwest Pacific basins to maintain hurricane structure and intensity to north of 40°N due to warmer water and a higher average latitude of the westerlies. North Atlantic hurricanes do not encounter the equatorward flank of the climatological westerlies until 30°N (Fig. 5c) and benefit from water temperatures above 26°C as far north as 37°N (Fig. 5d). Hart and Evans (2001) noted that transitioning North Atlantic storms retained their distinctive hurricane structure until an average latitude of around 40°N.

b. Influence of ENSO

Tracks for the 81 storms that made it south of 35°S are shown in Fig. 6. Clearly, storms can enter middle latitudes anywhere between the Australian coast and about 130°W. However, it is well known that the phase of the El Niño–Southern Oscillation (ENSO) cycle exerts a marked influence on the distribution of TCs (Nichols 1984; Revell and Goulter 1986a,b; Hastings 1990; Basher and Zheng 1995). Figures 6b and 6c indicate how ENSO impacts the regions where transitioning storms enter extratropical waters. During El Niño conditions (SOI < -1), most of the 22 storms enter middle latitudes east of the dateline, with nearly all storms exhibiting strong zonal motion. Calculations (not shown) for the tracks in Fig. 6b revealed an average storm motion toward the ESE in excess of 10 m s^{-1} in the region south of 30°S. However, during La Niña (SOI > 0.5) conditions (Fig. 6c), most of the 19 instances of TCs moving south of 35°S occur west of the dateline, with average storm motion south of 30°S toward the south or SSE at an average speed of just 7 m s^{-1}.

The influence of ENSO on average storm intensity is

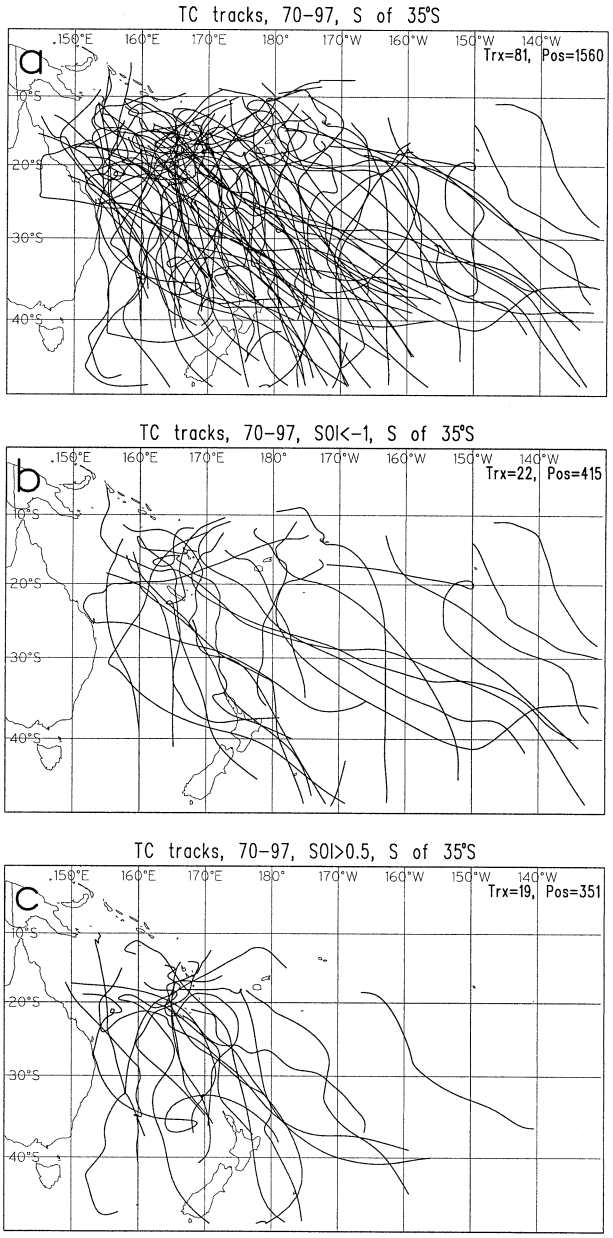

FIG. 6. (a) Tracks for all tropical cyclones progressing south of 35°S. (b) As in (a) except during periods where SOI < -1. (c) As in (a) except during SOI > 0.5.

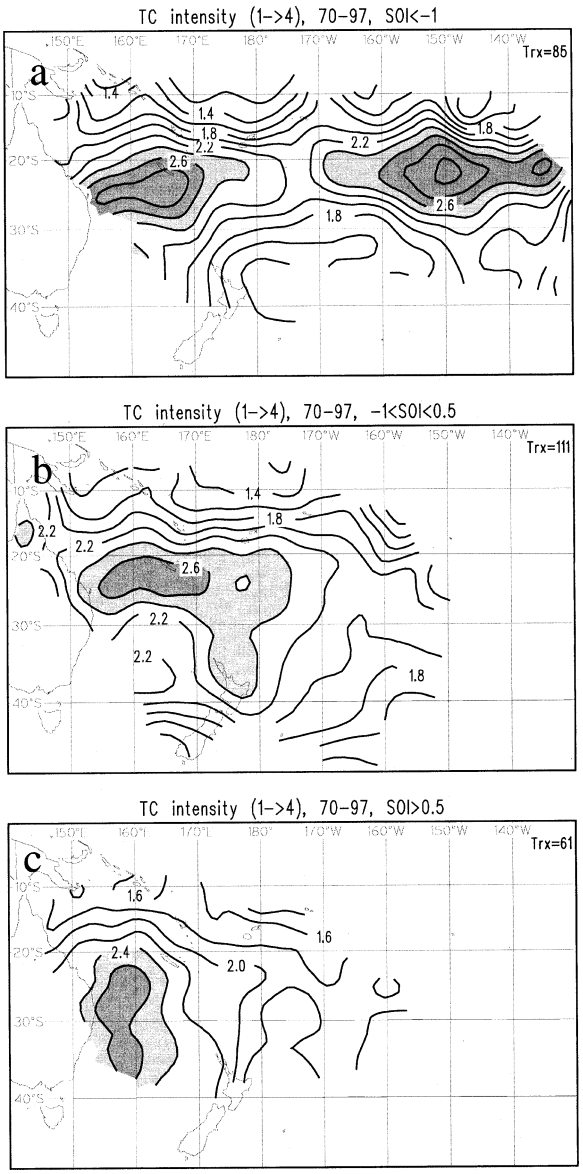

FIG. 7. Average tropical cyclone intensity for (a) SOI < -1, (b) $-1 <$ SOI < 0.5, (c) SOI > 0.5. Contours are every 0.2 intensity units, with values above 2.4 and 2.6 shaded.

shown in Fig. 7, based on the population of 251 storms since 1970 and for three ENSO categories. Intensity averages are normalized by the number of track points for each storm. This avoids bias favoring slower-moving or longer-lived storms and estimates the most likely intensity for a storm at each location. During El Niño conditions (Fig. 7a), intensity occurs in a fairly zonal pattern that decreases rather rapidly south of twin maxima straddling the dateline near 20°–25°S. Clearly, storms making it poleward of 30°S during El Niño months weaken much more rapidly compared with other ENSO categories (Figs. 7b,c). During La Niña months (Fig. 7c), storms retain intensity >2.4 (shaded) almost to 40°S in the Tasman Sea, with average intensity decreasing toward the east. However, during intermediate conditions ($-1 <$ SOI < 0.5), a lobe of maximum intensity extends toward NZ (Fig. 7b). Thus, TCs directly impacting NZ have their greatest intensity during near-zero SOI.

To understand the impact of ENSO on TC motion and intensity, atmospheric circulation and SST anomaly composites were examined for opposite phases of ENSO (Fig. 8). During El Niño, westerlies are stronger than normal over most of the subtropical region about and east of NZ (Fig. 8a), consistent with the more zonal TC

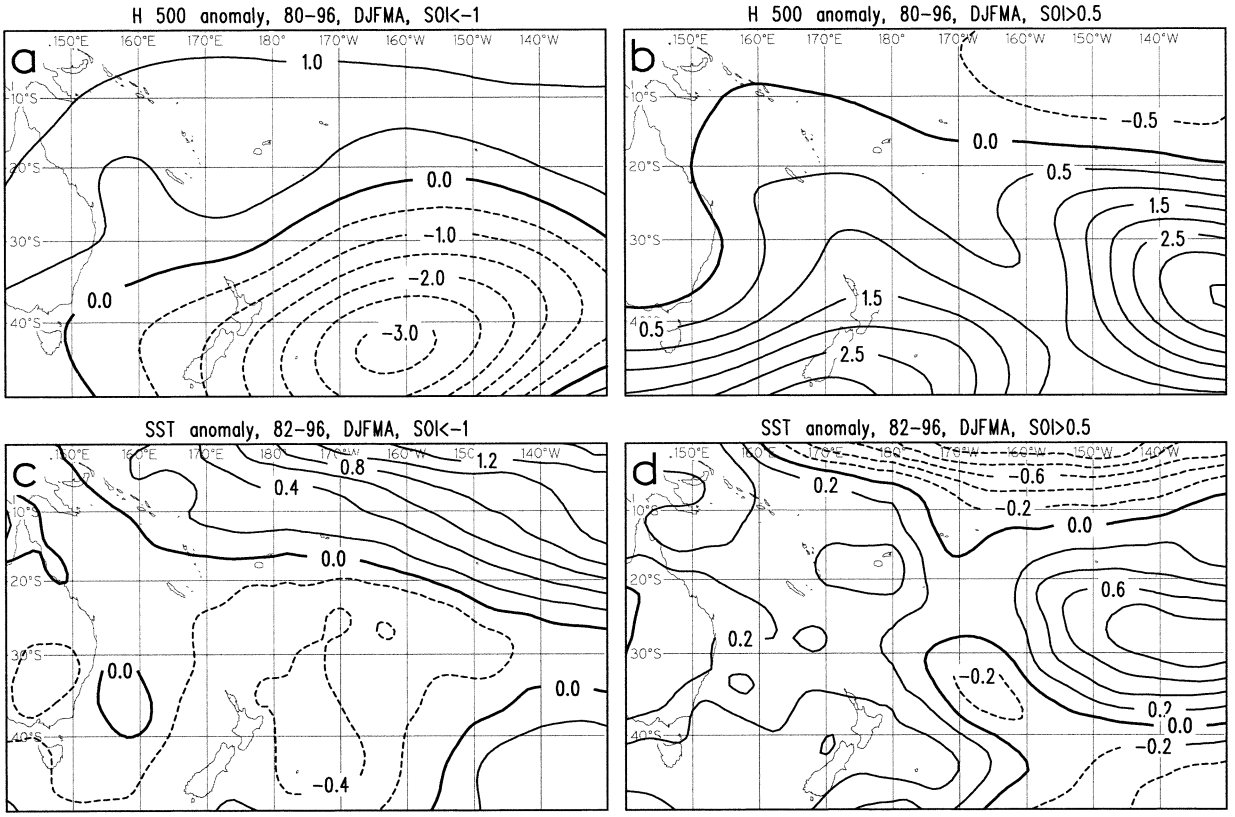

FIG. 8. Composite 500-hPa-height anomalies, every 0.5 dam for Dec–Apr for (a) SOI < -1 and (b) SOI > 0.5. (c), (d) As for (a), (b) except SST, every 0.2°C.

tracks in Fig. 6b. During La Niña periods, westerlies are weaker (Fig. 8b), with more meridional TC motion (Fig. 6c). Warm SST anomalies are found north of about 20°S during El Niño (Fig. 8c), especially in the east of the region, explaining the increased occurrence and intensity of TCs over tropical waters east of the dateline (Figs. 6b and 7a). The tendency for TCs east of NZ to weaken rapidly during El Niño (Fig. 7a) is possibly due to the cool anomaly in this region. La Niña SST composites (Fig. 8d) revealed cool anomalies along the equator, with small warm anomalies near and west of NZ longitudes, consistent with the greater occurrence and intensity of ET in these longitudes.

c. Influence of SST

To identify the importance of SST in determining the strength of transitioning storms, in situ concurrent gridpoint SST (Reynolds 1988) and monthly SST anomalies were correlated with intensity of the 81 transitioning storms (Table 3). In the far north of the domain, storm intensity is negatively correlated with SST, while south of 30°S it is positively correlated. These relationships merely reflect the fact that average storm motion is toward the pole (Fig. 3b), with average TC intensity peaking near latitude 20°–25°S (Fig. 3c). Cyclones north of 20°S intensify on average as they move south over cooler water, then weaken farther south. Clearly, factors other than SST determine the location of average maximum intensity.

Of more interest are correlations with SST *anomalies* (third column of Table 3), computed at each cyclone location from gridpoint SST data as monthly departures from the long-term mean. These correlations are smaller than with raw SST. The only relations statistically significant at the 5% level are a small negative correlation between storm intensity and SST anomalies north of latitude 20°S and an even weaker positive correlation south of 30°S. This negative correlation in the Tropics is at first surprising. Basher and Zheng (1995) and others have noted a negative correlation with SST anomalies

TABLE 3. Correlation of storm intensity (I) with SST and monthly SST anomaly. Only correlation coefficients significantly different from zero at the 5% level are included.

Latitude range	I vs SST	I vs SST anomaly	No. of points
0°–15°S	−0.35	−0.28	103
15°–20°S	−0.15	−0.15	177
20°–30°S	—	—	183
30°–90°S	+0.42	+0.15	190

for some regions, which they attributed to a negative feedback on SST through the cooling effect of a more active cyclone season on the ocean. A similar effect is probably seen here, with more intense storms contributing to greater mixing and cooling in the ocean.

South of 30°S, the small positive correlation (0.15) of *I* with SST anomalies suggests that storms moving into middle latitudes exhibit a slight tendency to be more intense when moving over warmer than normal water. However, as SST anomalies explain little more than 2% of the total variability in storm intensity, it is concluded that transient atmospheric circulation factors exert the dominant control on the vigor of an individual ET event.

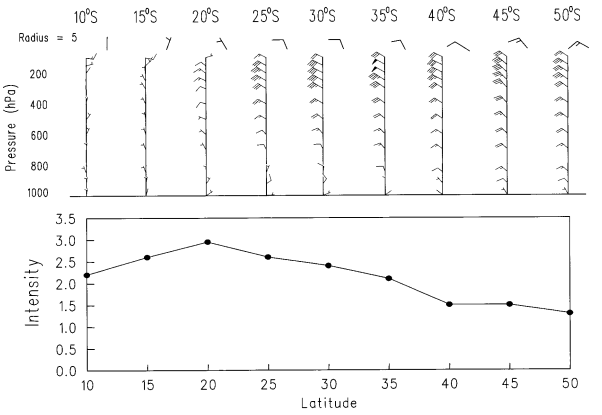

FIG. 9. (top) Winds, vector averaged over a 555-km-radius circle centered on each storm and composited as a function of latitude, in kt (1 kt = 0.514 m s^{-1}), with one full (half) barb equal to 10(5) kt and one pennant equal to 50 kt. (bottom) Storm intensity in the Table 1 intensity units plotted as a function of latitude.

4. Extratropical transformation

a. Composite NCEP diagnostics

This section describes how the average structure of southwest Pacific TCs changes as the TCs move into middle latitudes. As these storms encounter the baroclinic westerlies and cooler SSTs early in their life, extratropical transformation commences at lower latitudes (20°–25°S) than their NH counterparts. Demise of the symmetric hurricane structure comes about as thermal advection associated with increasing baroclinity brings cooler and drier air into the western sector of the storm, inhibiting convection there (Muramatsu 1985; Sinclair 1993a; Klein et al. 2000). The storm progressively acquires asymmetries characteristic of midlatitude frontal cyclones as it advances into the midlatitudes. Details of the process for one southwest Pacific ET event are illustrated in Sinclair (1993a).

Composite diagnostics are used to illustrate typical structure changes as southwest Pacific TCs move into middle latitudes. NCEP data from a subset of 33 storms (653 12-h track points) that progress poleward of 35°S between 150°E and 170°W after 1980 are used. The year 1980 corresponds to the start of the modern satellite era, a period of increased data coverage over the SH (Kistler et al. 2001). Storms east of 170°W were not considered because analysis quality there is still reduced by limited observational data. Compositing follows Sinclair and Revell (2000), and is performed on a 31 × 31 Lambert conformal domain 3330 km × 3330 km in size (about 1° by 1° latitude) that is exactly centered on the TC center coordinates as read from the cyclone database.

Average vertical profiles of various vector quantities over the storm environment composited by latitude (Fig. 9) illustrate some of these changes. Stratification by latitude is justified in view of the zonal symmetry of the time-averaged SH circulation (Fig. 5). First, vector averages of NCEP winds at each level are constructed over a 5° latitude (555-km) radius circle centered on each storm's maximum 1000 hPa cyclonic vorticity. Vertical profiles of these vector quantities are then constructed for a composite (average) for all cyclones centered within 2.5 degrees of each 5° latitude value. Fields are interpolated onto the 1° × 1° compositing grid prior to averaging. To avoid bias favoring slow-moving storms, each storm is included just once for each latitude, with the position chosen being the one closest to the 5° latitude value. Average storm motion and intensity by latitude is also included in Fig. 9.

In the 10°–20°S latitude band where hurricanes move slowly south on average while intensifying, circle-averaged vector magnitudes are mostly below 5 m s^{-1}. According to Table 1, average storm winds at this stage are in excess of 25 m s^{-1}. Although analysis resolution hampers accurate depiction of these strong inner core winds, analyzed average circular flow remains much in excess of the vector averages in Fig. 9. Thus, these small vector averages reflect the high degree of storm symmetry rather than a lack of storm wind. A stationary symmetric vortex would exhibit a vector average of zero. At maximum average hurricane intensity near 20°S, upper-level westerlies are already affecting the storm, suggesting an onset of baroclinic characteristics even at this early stage. This is consistent with Fig. 5a, which shows climatological westerlies all the way to 15°S. South of 20°S where average storm intensity starts to weaken, vertical shear and asymmetry increase, mostly above 500 hPa, as the composite storm approaches then crosses the upper troposphere westerly wind maximum near 35°S. Average vector winds remain small below about 500 hPa, attesting to greater vortex symmetry in the middle and low troposphere. Average storm motion is at first toward the south followed by gradual acceleration toward the southeast, consistent with Fig. 3b.

The picture here is of increasing upper winds blowing across the top of a vortex as it moves into middle latitudes. This results in shearing off to the east of the characteristic symmetric hurricane cirrus cloud shield, as illustrated in several images in Klein et al. (2000) and for one southwest Pacific cyclone (Patsy) in Sin-

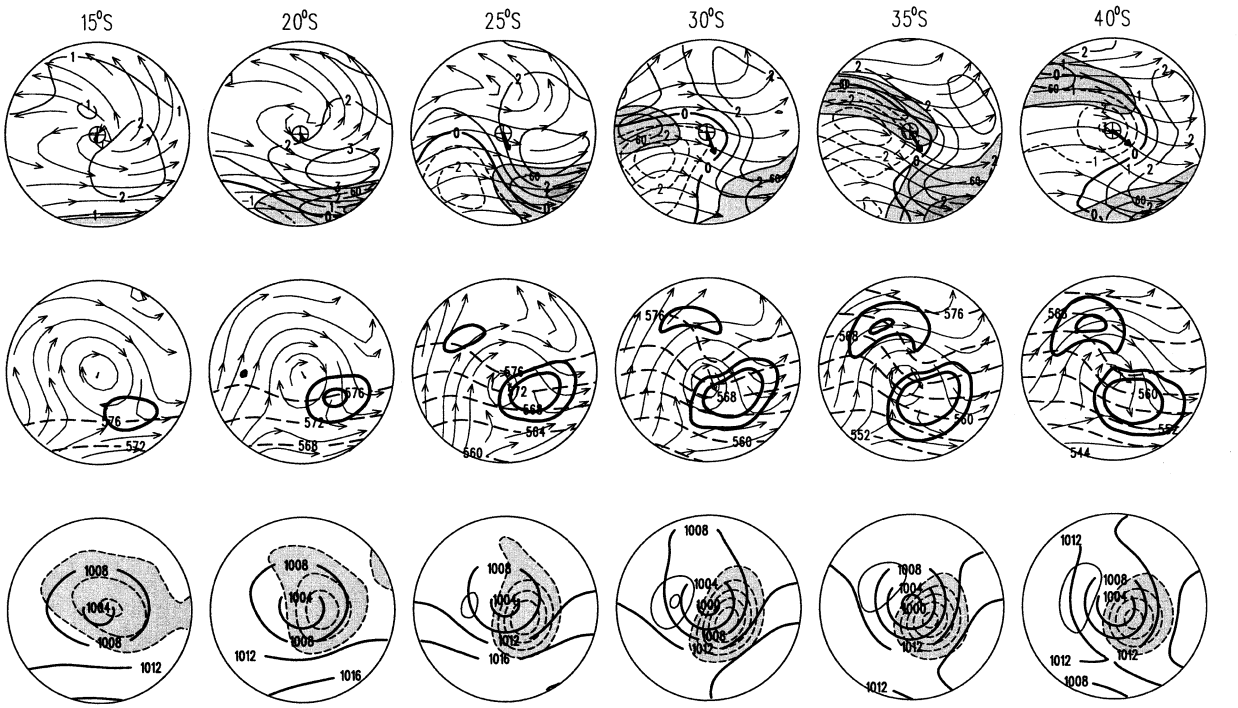

FIG. 10. Composite fields as a function of latitude (indicated at the top of each column) over 1667-km-radius circles centered on the composite storm. (top row) 200-hPa streamlines, isotachs (every 5 kt from 55 kt, values >65 kt shaded), and relative vorticity (every 1×10^{-5} s^{-1}), with positive (negative) values thin solid (dashed), zero thick solid. (middle row) Streamlines at 500 hPa, 1000–500-hPa thickness (every 4 dam, dashed) and the 2 and 5 K $(10^3$ km$)^{-1}$ day^{-1} contours of 850 hPa frontogenesis (heavy solid). (bottom row) MSL pressure (every 4 hPa, solid), 700 hPa vertical P-velocity, ω, every 2 hPa h^{-1}, with positive (negative) values thin solid (dashed) and the zero contour omitted. Ascent regions ($\omega < -2$ hPa h^{-1}) are shaded.

clair (1993a). On average, this destruction of the symmetric hurricane structure commences in the 20°–25° latitude band, much sooner (i.e., at a lower latitude) than in the NH.

b. Composite maps during ET

Details of the changes in storm structure are identified using composites of various fields in 5° latitude bands (Fig. 10). The maps in Fig. 10 comprise storm-relative streamlines and relative vorticity aloft (top row), 500 hPa streamlines with the 1000–500 hPa thickness and frontogenesis added (middle row), and MSL pressure and vertical motion fields (bottom row). Frontogenesis (heavy contours) is computed at 850 hPa using the Petterssen (1936) formulation for horizontal adiabatic motions, namely

$$\frac{d}{dt}|\nabla_p\theta| = \frac{1}{2}|\nabla\theta|(E\cos 2\beta - \nabla\cdot\mathbf{V}) \qquad (1)$$

where β is the angle between isentropes and the axis of dilatation, $\mathbf{V}$ is the horizontal velocity vector, and E is the magnitude of the total deformation, $E = (E_{st}^2 + E_{sh}^2)^{1/2}$, where $E_{st} = \partial u/\partial x - \partial v/\partial y$ and $E_{sh} = \partial v/\partial x + \partial u/\partial y$.

These maps confirm the earlier picture proposed from Fig. 9. At 15° and 20°S, the composite, slow-moving mature hurricane exhibits the expected near-symmetric anticyclonic upper-level outflow pattern overlying a near-circular cyclonic vortex at 500 hPa and below. Extratropical transition proceeds as an upper trough approaches from the west. As the storm progresses south, the symmetric outflow pattern shows a preference for outflow into the confluent equatorward entrance region of a downstream upper-level jet located to the southeast. Strong anticyclonic vorticity appears between the cyclone and the equatorward flank of this jet. The symmetric outflow pattern is progressively channeled into this downstream jet and eventually replaced by strengthening upper-level westerlies and cyclonic vorticity advection (CVA) aloft along the equatorward flank of the jet entrance. By 30°S, a second upper-level wind maximum appears to the west and migrates into the region northwest of the storm center, augmenting the CVA and making the environment above the storm progressively more cyclonic. The composite storm continues to move

southeast beneath this double upper jet signature. This double jet structure is similar to that observed by Sinclair (1993b) for Cyclone Bola and by DiMego and Bosart (1982a,b) for Agnes, and is known to favor tropospheric ascent through mutual reinforcement of the associated vertical circulations (Uccellini and Kocin 1987).

Flow patterns at 500 hPa (middle row of Fig. 10) feature a nearly circular warm-cored closed cyclonic vortex migrating into increasing midlatitude baroclinity, with strengthening warm advection to the east and cold advection to the west. Even at 15°S, proximity to the baroclinic westerlies results in frontogenesis in the warm advection region southeast of the center, in the deformation region between the vortex and the westerlies. This frontogenesis occurs beneath the lobe of anticyclonic vorticity located along the equatorward flank of the downstream upper jet (top row). As the storm moves south into the baroclinic westerlies, this warm-front-like region intensifies and expands. By 25°S, a second weaker area of frontogenesis develops via differential thermal advection near the trough to the northwest of the center, directly beneath the upstream upper-level jet. During ET, the cyclone center remains warmer than its surroundings all the way to 50°S (not shown but similar to 40°S).

The patterns of frontogenesis are similar to those identified by Klein et al. (2000) and Harr and Elsberry (2000) for western North Pacific ET events. They found warm frontogenesis to dominate over weaker cold frontogenesis, with precipitation chiefly observed in conjunction with the warm front. The southwest Pacific cases presented by Sinclair (1993a,b) and included in the composites, also showed the most active multilayered cloud and heavy precipitation in the warm frontal region in the poleward and eastern sector, but only weaker cold frontal cloudiness. A strong warm front is consistent with the generally confluent nature of the upper-level flow. Sawyer (1950) first noted that cyclones possessing stronger warm fronts tended to form in confluent flow near jet entrances. Schultz et al. (1998) and others proposed that cyclones evolving within a confluent environment acquire stronger warm fronts and evolve according to the Shapiro–Keyser model (Shapiro and Keyser 1990), with perpendicular cold and warm fronts, a feature observed in Harr and Elsberry (2000). Sinclair and Revell (2000) found that several southwest Pacific midlatitude cyclones developing beneath confluent airflow aloft also went on to form stronger warm fronts and weaker cold fronts.

Composite sea level pressure and vertical *P*-velocity fields are shown in the bottom row of Fig. 10. Ascent, initially centered more or less on the storm, migrates rather quickly to the eastern sector, so that at maximum intensity near 20°S, ascent is already displaced slightly to the east where upper-level CVA exists. The magnitude of this ascent reaches a maximum at about 30°S, then wanes a little. Ascent occurs beneath the CVA region along the equatorward entrance region of the upper jet, which is later complemented by the second upstream jet. From about 30°S poleward, ascent occurs in the region where the CVA aloft occurs in phase with warm advection, as analyzed in detail by Sinclair (1993b) for one of the storms in the composite set. Vigorous mesoscale ascent associated with the mature hurricane north of 25°S is clearly underestimated by this course-resolution dataset and by the averaging. As the composite storm advances poleward, weaker descent appears in the western sector. Relative humidity (RH) analyses (not shown), which only extend to 300 hPa in the NCEP analyses, show highest RH matching the ascent in the low and middle troposphere, with drier air to the west. At 300 hPa, however, a tongue of high RH extends southeast of the storm, in the region where downstream shearing of the cirrus cloud shield is often observed in satellite imagery.

c. Composite cross sections

East–west cross sections are shown in Fig. 11. At 15°S (and 20°S, not shown), a ''tower'' of cyclonic vorticity extends to 200 hPa, with anticyclonic outflow above and on either side in the anticyclonic environment there. Maximum cyclonic vorticity is found near 900 hPa, just above the surface layer. Close examination reveals that the vorticity tower slopes very slightly to the west at this stage. Wind barbs depict the symmetric outflow above 200 hPa and the cyclonic vortex at lower levels. Clearly, these winds underestimate the intensity of the inner core circulation. Ascent (shaded) and highest wet-balb potential temperature θ_w (bottom row) are almost centered on the storm at this stage, with ascent maximizing near 300 hPa. The atmosphere is convectively (potentially) unstable below the solid line (about 600 hPa).

As the composite storm moves poleward (25° and 35°S), the diffluent anticyclonic outflow above 200 hPa is replaced by increasing westerlies blowing through the top of the storm. Cyclonic vorticity aloft increases west of the center and eventually extends all the way to 100 hPa, making the tower of cyclonic vorticity tilt westward (upshear) with height above about 400 hPa. At the same time, the upper tropospheric warm core moves east of the center, resulting in a downshear tilt in maximum θ_w. A similar downshear tilt in potential temperature was noted by Klein et al. (2000) during the ET of Typhoon David and observed in idealized simulations of ET (Frank and Ritchie 1999).

The upshear tilt in vorticity observed here during ET appears to differ from shear effects observed in NH ocean basins and in idealized modeling studies. Numerical simulations by Frank and Ritchie (1999) showed that the introduction of vertical shear induces a downstream tilt in both maximum potential temperature *and* PV. These features were observed during early stages of ET by Klein et al. (2000) for Typhoon David, and

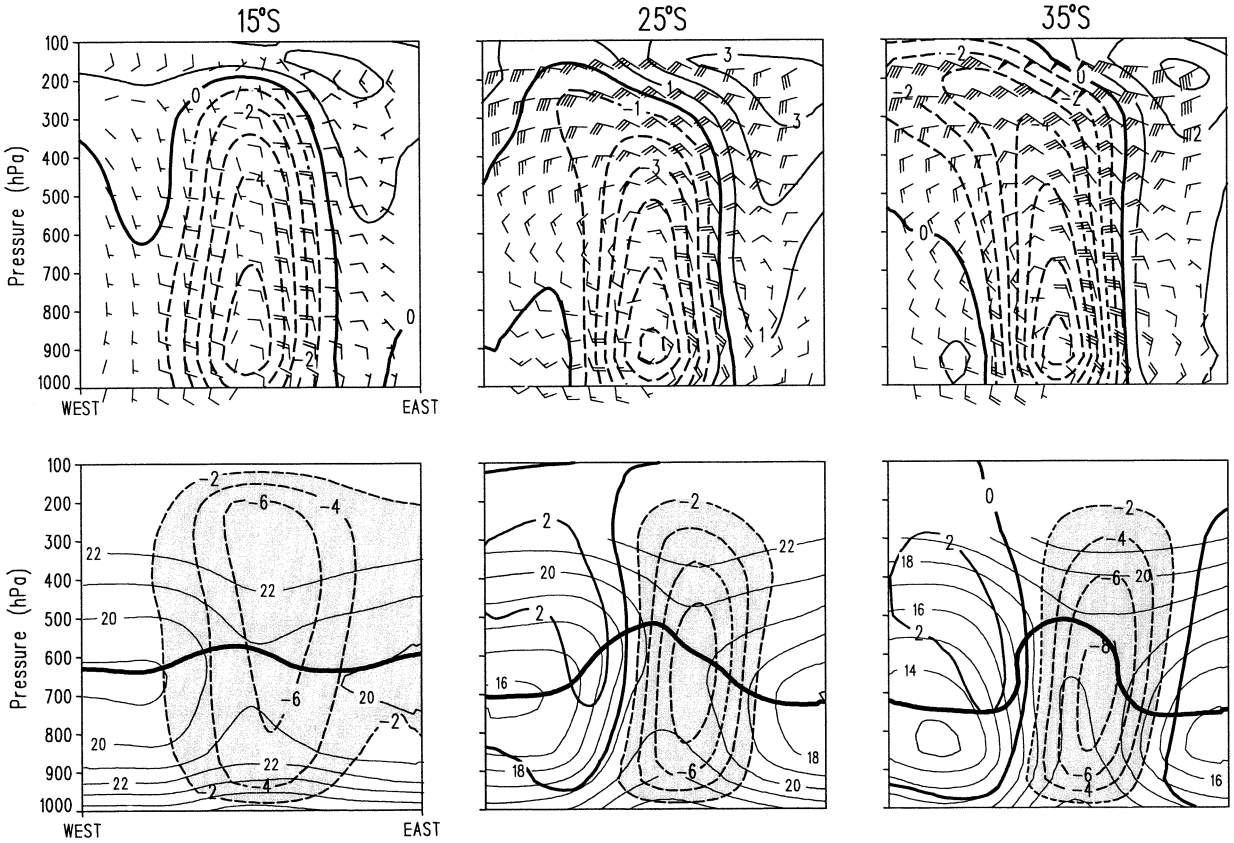

FIG. 11. Composite vertical west to east cross sections extending 1667 km either side of the composite storm center. (top row) Relative vorticity, every 1×10^{-5} s^{-1}, showing positive values (thin solid), negative values (dashed), and zero (thick solid); and horizontal wind (kt). (bottom row) Wet-bulb potential temperature, θ_w (every 1°C, thin solid); vertical P-velocity ω every 2 hPa h^{-1}, showing positive values (thin solid), negative values (dashed), the zero contour (solid), and ascent regions $\omega < -2$ hPa h^{-1} (shaded); and the zero contour of $\partial\theta_w/\partial p$ (heavy solid).

Thorncroft and Jones (2000) for Hurricane Iris over the North Atlantic. However, Jones (1995) showed that TC-like vortices in vertical shear undergo structural changes that depend on the strength of the shear and the size and intensity of the vortices, and that there is not always a simple relationship between the direction of the shear vector and the direction of the vortex tilt. Separate east–west cross sections of PV (not shown) suggest a very slight eastward tilt of PV at 15° and 20°S, changing to a westward tilt from 25°S southward, similar to the evolution of the vorticity tower in Fig. 11 (top row). It is probable that tilting effects are blurred here by the coarse resolution and the compositing. For example, totally separate upper PV anomalies to the west from approaching short-wave troughs may be merged by the averaging, giving the false appearance of a westward tilt. However, taking the vorticity profiles in Fig. 11 at face value suggests that any eastward tilt is minimal and only evident at early stages, and changes to a westward tilt by 25°S as the TC interacts with the baroclinic westerlies. Extratropical transition in the SH typically occurs as a TC becomes embedded in the poleward flow ahead of an approaching trough in the westerlies (Sinclair 1993a; Foley and Hanstrum 1994). The westward tilt and the development of secondary circulations in Fig. 11 suggest baroclinic coupling between this approaching trough and the TC (Fig. 10) from at least 25°S poleward. Low- and midlevel thermal advections accompanying the cyclonic vortex produce warming east of the center and cooling west of it, making the upper-level flow progressively more cyclonic to the west and fostering the observed upstream tilt in vorticity. It is suggested that the downshear PV tilt, observed as far poleward as 40°N in NH studies, is probably only observed equatorward of about 25°S in the southwest Pacific.

Below about 500 hPa, greater symmetry is maintained in both the vorticity and thermal structure as the storm moves poleward (25° and 35°S), with the warm cyclonic core of highest θ_W maintaining a near-vertical structure near the center of the storm (bottom row of Fig. 11).

However, maximum ascent shifts east of the surface center and lowers to around 700 hPa. The level of minimum θ_W lowers to near 800 hPa, with a deeper layer of potential instability found only within the warm core. West of the storm, θ_W is about 2°C cooler than to the east, consistent with the amplifying thermal trough west of the center (Fig. 10). Values of θ_W below 13°C at 35°S suggest that cooler and drier midlatitude air is being incorporated into the low-level circulation.

Various hypotheses have been put forward to explain the maintenance of the warm core. Thorncroft and Jones (2000) and Browning et al. (1998) identified a persistent warm core for some North Atlantic ET events. In these cases, the ''capture'' of the warm core was attributed to the midlatitude PV intrusion wrapping cyclonically around the decaying tropical cyclone, in a manner similar to the seclusion process described by Shapiro and Keyser (1990). Unfortunately, present analysis resolution is too coarse to identify this process. Convection near the decaying cyclone center can also help to maintain a warm core, with continued convection aided by a favorable track over warm water. Core convection is suggested by the deeper layer of convective instability near the storm core (Fig. 11), and by the near-saturation in the core region (not shown). Here, as in other ocean basins, cyclones move over progressively colder SSTs (Fig. 5b) during ET. Despite this, the high θ_W warm core and convectively unstable air in Fig. 11 extend all the way to the surface, suggesting that the warm core remains coupled with the underlying sea. Values of θ_W decrease simultaneously at all levels during ET as the poleward-moving TC adjusts to lowering SSTs. This is similar to the convective coupling noted by Thorncroft and Jones (2000) during the ET of Hurricane Iris. Felix, on the other hand, formed a stable surface layer via negative fluxes resulting from rapid motion toward much colder water, with the warm core persisting only above about 850 hPa. Here, slower average poleward movement across more modest SST gradients (Fig. 5) makes formation of a surface stable layer appear less likely. Future work involving more cases is needed to establish if there is a systematic connection between the rate of motion across SST isotherms and the formation of a stable surface layer and suppressed convection.

Warm core longevity may also be associated with a long spindown time for the intense low-tropospheric cyclonic core left over from the hurricane as it migrates poleward over progressively cooler oceans. Relatively straight upper-level flow across a rapidly spinning low-level cyclonic vortex as depicted in Figs. 10 and 11 hydrostatically implies a warm core structure. Where a poleward-moving cyclone decouples from the ocean, lengthened spindown times may also aid persistence of the warm core above the stable surface layer.

d. The downstream jet

Two upper jet streaks and frontogenesis patterns occur in association with extratropical transformation in the southwest Pacific—one downstream, and a second appearing later on the upstream side (Fig. 10). We first examine the role of the downstream jet. Holland and Merrill (1984) proposed that intensification of hurricanes in the Australian and southwest Pacific regions occurs via a strengthening of the poleward outflow channel as the TC approaches the downstream subtropical jet (STJ), as depicted in Fig. 12. They suggested that strengthening occurs when a STJ passes 600–800 km poleward of the hurricane, reducing the already low inertial stability in the outflow region and generating a divergent area poleward and eastward of the cyclone center. This coupling is typically of short duration and ceases when the trough either moves away to the east, cutting off the outflow channel, or the westerlies move right over the cyclone, resulting in decay from shearing effects. This scenario was hypothesized as a mechanism for hurricane intensification prior to ET.

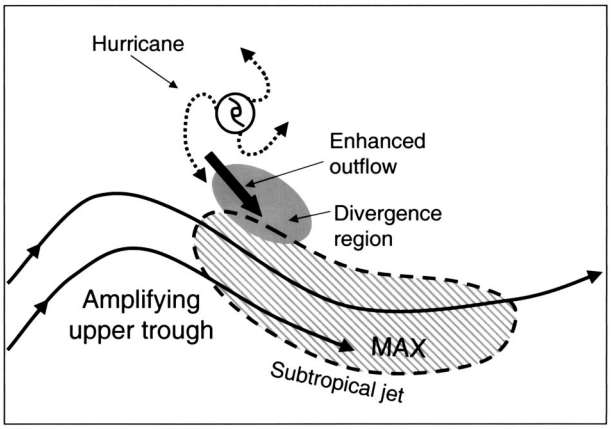

FIG. 12. Illustration of the manner in which the subtropical westerlies and a cyclone may interact to produce a poleward outflow channel (after Holland and Merrill 1984).

Figure 10 shows that the composite downstream outflow jet moves poleward with the storm during ET, implying a more prolonged period of coupling with the downstream jet than in the scenario for hurricane intensification proposed by Holland and Merrill (1984). Examination of individual upper air plots for the thirty cases showed that the downstream jet remains locked in the same position relative to the poleward-moving cyclone during ET in about half the ET cases. This is illustrated in Fig. 13 for one storm, TC Fergus (December 1996), which shows the downstream jet migrating south with the storm over a period of at least 3 days. Strongest anticyclonic vorticity occurs southeast of the center (see also Fig. 10) along the equatorward flank of the downstream jet, which strengthens as it moves poleward with the storm (Figs. 13a–d). Following Elsberry et al. (1987), an inertial stability parameter is computed as $(\zeta_r + f)(2\mathbf{V}/r + f)$, where ζ_r is the relative vorticity, f is the Coriolis parameter, $\mathbf{V}$ is the horizontal velocity vector, and r is the radius of curvature. Regions of inertial instability are contained within the heavy black contours

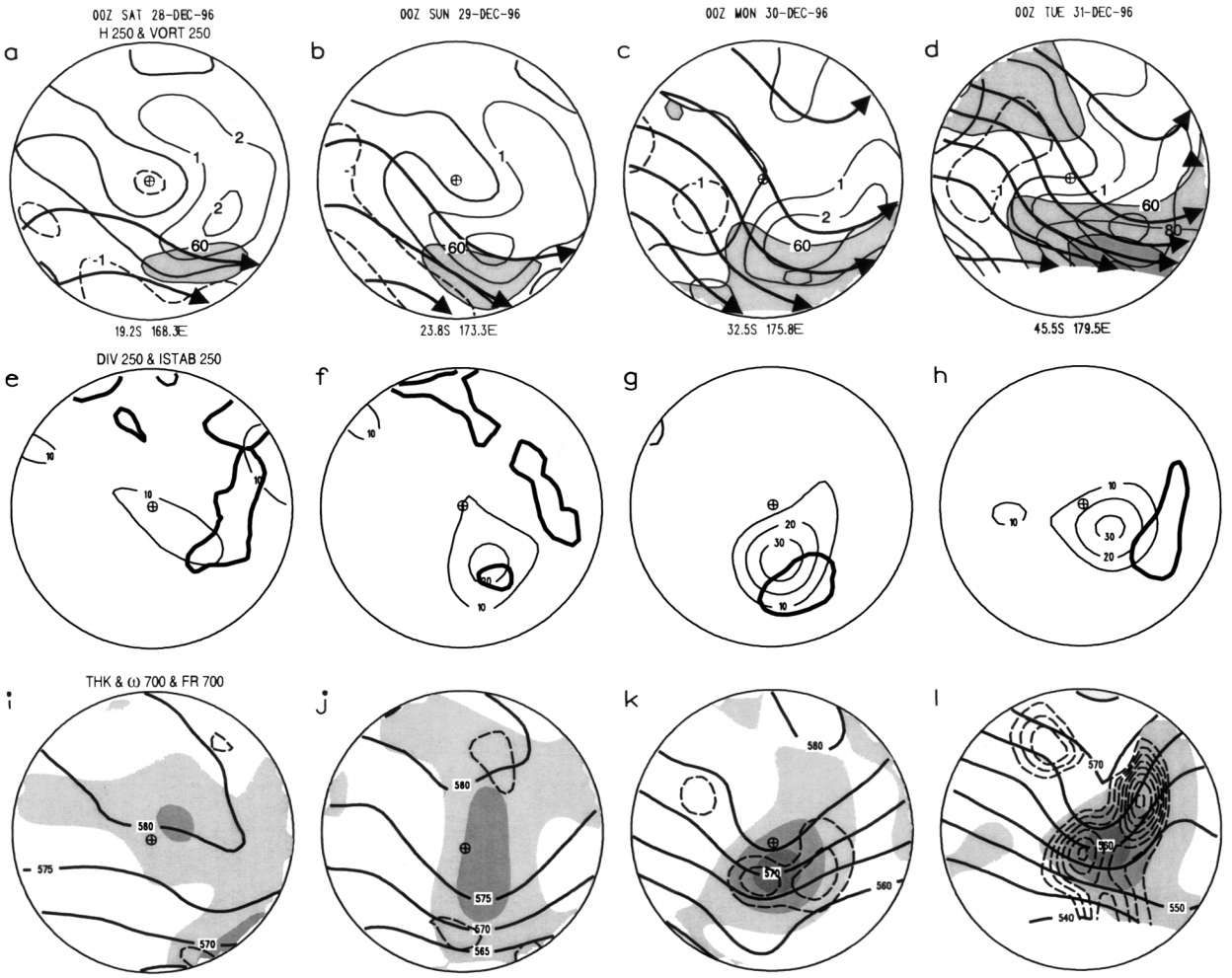

FIG. 13. (a)–(d) 250-hPa geopotential, every 10 hPa (solid, with arrows showing direction of geostrophic flow); 250-hPa vorticity, every 1×10^{-5} s^{-1}, showing positive values (thin solid), negative values (dashed), and zero (solid); and isotachs, contours every 10 kt above 60 kt, with shading at 60 and 90 kt. (e)–(h) 250-hPa divergence, every 10×10^{-6} s^{-1} (thin solid), and the zero contour of inertial stability (thick solid). (i)–(l) 1000–500-hPa thickness, every 5 dam (solid); 700-hPa frontogenesis, contours every 2×5 K $(10^3$ km$)^{-1}$ day^{-1} starting at 2 (dashed); and ascending 500-hPa vertical *P*-velocity (shaded), with shading for -2, -5, and -10 hPa h^{-1}. Some contour labels have been omitted for clarity.

in Figs. 13e–h. These regions are approximately collocated with maximum anticyclonic vorticity in the region where air is accelerating into the downstream jet. Other inertially unstable regions are found northeast of the center, possibly associated with equatorward outflow. Inertial instability persists along the equatorward flank of the upper jet as Fergus moves poleward into middle latitudes, favoring continued strong upper-level divergence. Maximum divergence occurs just upstream of the region of inertial instability, in the region where air accelerates into the downstream jet.

Another factor favoring 250-hPa divergence is the anticyclonic environment in which the CVA is occurring. The vorticity equation in storm-following coordinates is

$$\frac{\delta\zeta}{\delta t} \approx -(\mathbf{V} - \mathbf{C}) \cdot \nabla(\zeta + f) - (\zeta + f)\nabla \cdot \mathbf{V}, \quad (2)$$

where ζ is the relative vorticity and other symbols have their usual meanings. Here, $\delta/\delta t$ is the change following the storm, moving with velocity **C**. Vertical advection and twisting terms have been omitted, as they are typically an order of magnitude smaller than the other terms in coarse-resolution diagnostics (see Fig. 11 of Sinclair 1993a). Rearranging (2) yields an approximate expression for the divergence,

$$\nabla \cdot \mathbf{V} \approx \frac{-(\mathbf{V} - \mathbf{C}) \cdot \nabla(\zeta + f) - \delta\zeta/\delta t}{\zeta + f}. \quad (3)$$

Vorticity changes following the storm, $\delta\zeta/\delta t$ (the differences between the panels in Fig. 13) are typically small in comparison with the advection term according to vorticity budgets computed by Sinclair (1993a). Equation (3) suggests that strongest synoptic-scale divergence will be found where CVA is occurring near

an upper wind maximum ($\mathbf{V} \gg \mathbf{C}$), and that it will be enhanced where the CVA is occurring in an anticyclonic environment ($\zeta + f$ small) and where the flow is becoming more anticyclonic with time. This is consistent with the location of maximum divergence (Figs. 13e–f) and ascent (Figs. 13i–l) close to the upper ridge. Frontogenesis at 700 hPa, computed from (1), and thickness (Figs. 13i–l) reveal a strengthening baroclinic zone south and southeast of the center in the region below the upper jet, consistent with the observed strengthening of the upper jet.

It is suggested that the downstream jet migrates poleward with the cyclone because of a synergy between the upper jet and the frontogenesis, ascent, and heating fields of the cyclone. As the TC migrates into the baroclinic westerlies, tropospheric frontogenesis commences southeast of the center (Figs. 10 and 13i–l). This enhances the upper jet and maintains low absolute vorticity and inertial instability along its equatorward flank (Fig. 13). Reduced absolute vorticity favors increasing divergence close to the upper ridge via (3) and supports ascent that is able to tap warm, moist tropical air. Warming from latent heat release in the ascent region then helps maintain anticyclonic vorticity aloft. This warming may also contribute a diabatic frontogenesis component while strongest ascent remains on the warm side of the baroclinic zone, as in Fig. 13j.

The maintenance of the outflow jet as the storm moves poleward can also be viewed from an energy perspective. Generation and export of kinetic energy aloft east and poleward of the cyclone has been observed in previous studies of ET (Palmén 1958; DiMego and Bosart 1982b; Harr et al. 2000). Plots of 250-hPa winds and geopotential height (not shown) suggested marked generation and export of kinetic energy into the equatorward entrance region of the downstream jet as air flows across the height contours to lower geopotential. Harr et al. (2000) showed that about a third of the kinetic energy generation aloft for Typhoon David was associated with the velocity potential (divergence) maximum above the TC.

e. The upstream jet

An upstream jet appears in the composites from about 30° latitude and south (Fig. 10). Examination of individual charts from the 30 cases revealed that an upstream jet was present during later stages of ET in two-thirds of the cases. Of these, about half involved a separate jet that propagated into the area from the west while the remainder developed in situ just west of the surface low. An example of an in situ formation of an upper jet is TC Bernie, shown in Fig. 14. The upper jet strengthens northwest of the center (Figs. 14b,c) in response to a strengthening low-level circulation (Figs. 14d–f) that advects cold air equatorward west of the storm, increasing the baroclinity beneath the region of the upstream jet.

f. A conceptual model of extratropical transformation

Results are summarized with the aid of a conceptual model of southwest Pacific extratropical transformation (Fig. 15) based on the composite diagnostics. At maximum average intensity near 20°–25°S, the outer circulation of the mature, symmetric hurricane is already impinging on the equatorward flank of the baroclinic midlatitude westerlies, with strengthening outflow into a jet southeast of the center. This outflow is engendered by low inertial stability along the equatorward flank of the jet entrance region, and may temporarily assist the hurricane attain or maintain maximum intensity, as suggested by Holland and Merrill (1984). Thus, at 20°–25°S, Fig. 15 depicts the upper westerlies already encroaching on the poleward edge of the upper-level outflow and starting to deform the associated cirrus overcast toward the downstream jet while warm frontogenesis commences beneath the jet.

As the TC advances deeper into the midlatitudes, it loses its symmetric anticyclonic outflow as upper-level westerlies spread across the top of the storm, shearing off the upper anticyclone and associated cirrus cloud shield. This appears to occur at around 25°S. Although the storm has some baroclinic character right from the start, Fig. 10 reveals that from 25°S poleward, the TC acquires all the features of a midlatitude cyclone, including dipoles of cold (warm) advection, descent (ascent) and cold (warm) frontogenesis west (east) of the center, a westward tilt with height spreading CVA aloft over the center, and strengthening upper-level jets. Appearance of these asymmetries signifies that extratropical transformation has occurred, with the baroclinic character strengthening as the TC migrates farther into the westerlies. From this stage forward, the storm is a circular warm-cored vortex in the low to middle troposphere with westerlies blowing across the top. The system remains coupled with the downstream upper-tropospheric wind maximum that moves poleward with the storm (Fig. 13), a feature observed in at least half the storms studied. These storms continue to enjoy a synergy with the downstream jet during ET, with inertial instability and divergence along its equatorward flank helping the cyclone, while the jet is maintained by heating and tropospheric frontogenesis. A second 200-hPa-wind maximum with strengthening cyclonic vorticity and cold frontogenesis below appears in the western sector, increasing the CVA directly above the storm center. This upstream jet appears during ET in about two-thirds of cases. In about half the cases, it is an in situ response to strengthening cold frontogenesis (Fig. 14) as the storm migrates deeper into the baroclinic westerlies. In others, it is a separate feature that approaches from the west. Below 500 hPa, the storm retains the vertical, warm core, convectively unstable cyclonic vortex left over from the hurricane. This residual warm core structure persists well into the midlatitudes because

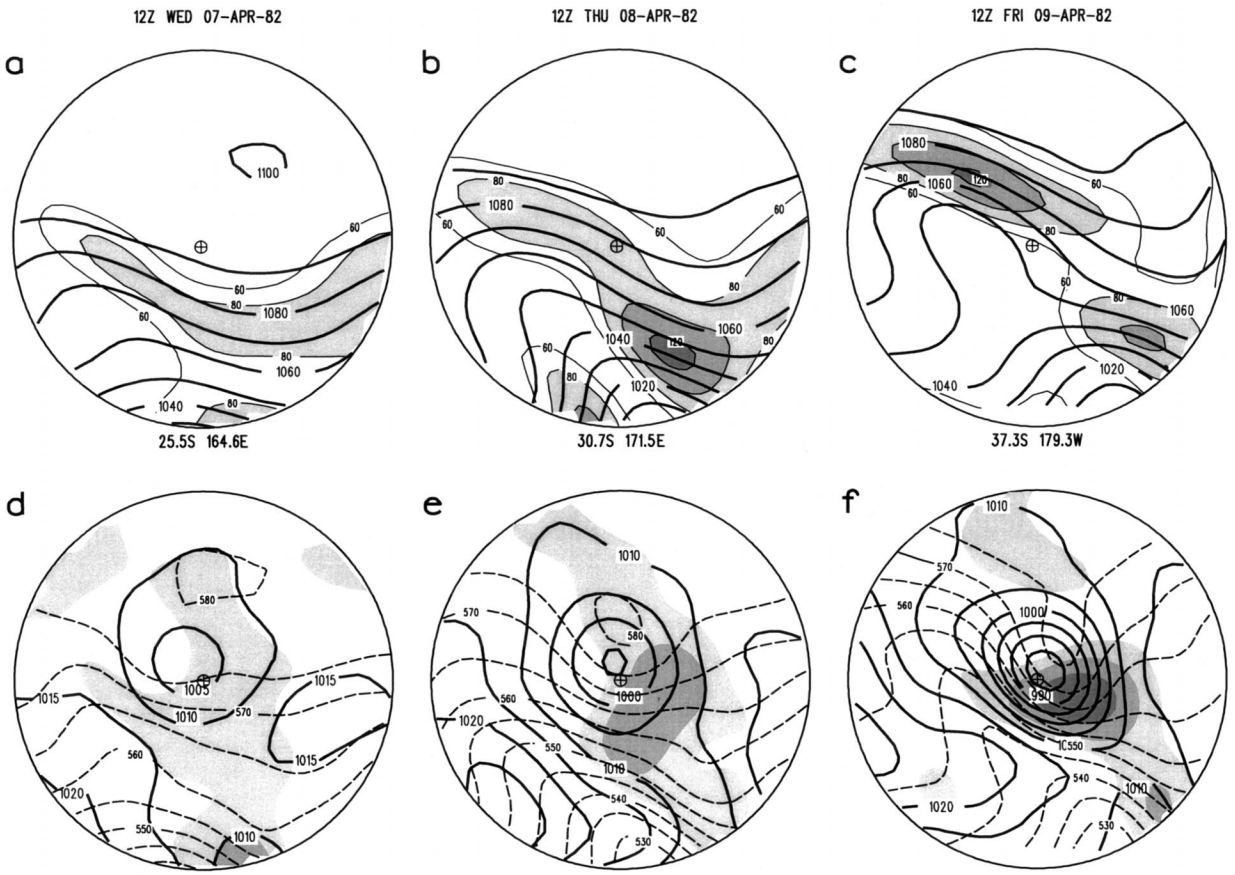

FIG. 14. (a)–(c) 250-hPa height, every 10 dam; and isotachs, every 20 kt starting at 60 kt, with values above 80, 100, and 120 kt shaded. (d)–(f) MSL pressure, every 5 hPa (solid); 1000–500-hPa thickness, every 5 dam (dashed); and vertical *P*-velocity ascent values below −2, −5 and −10 hPa h^{-1} (shaded).

of the modest SST gradients and the slow spindown time of the low-level vortex.

5. Summary and discussion

A database of tropical cyclone best track and intensity information has been used to construct a 28-yr climatology for tropical cyclones undergoing ET. Of the nine or so tropical cyclones that form each year, about a third can be expected to migrate south of 35°S, with the greatest fraction in March. Transitioning storms entering the Tasman Sea west of New Zealand move almost due south on average, occur earlier in the season and retain greater intensity than those to the east of NZ. There, storms decay quickly and move rapidly away to the southeast. During La Niña conditions, average storm motion is slower and more meridional than normal, with ET confined west of 170°W. During El Niño conditions, ET occurs throughout a wider range of longitudes between 160°E and 130°W, with faster and more zonal motion. Storm intensity during ET is only weakly correlated with concurrent SST anomalies, indicating that atmospheric circulation is the dominant influence on storm intensity.

Typical structure changes during ET are identified using gridded data from the NCEP-NCAR reanalysis dataset, for a subset of 33 transitioning storms during 1980–97 (Table 4). Composites for several latitude bands between 15° and 40°S are used to construct a three-dimensional conceptual model of the transformation from a mature hurricane to an asymmetric baroclinic midlatitude cyclone. A major conclusion from this study is that southwest Pacific tropical cyclones encounter the baroclinic westerlies early in their lives, accounting for their average eastward (and poleward) motion and early onset of extratropical transformation. At hurricane maturity near 20°S, warm frontogenesis is already evident in the southeast quadrant, while aloft, the anticyclonic outflow starts to deform toward a subtropical wind maximum to the southeast. Between 20° and 25°S, the cyclone commences weakening as upper-level westerlies spread across the top of the storm, shearing the cirrus shield off to the southeast and tilting strongest ascent to the east. From 25°S poleward, the storm has all the characteristics of a midlatitude storm, including asymmetric thermal and vertical motion fields, upper jets, cold and warm frontogenesis regions, and a westward tilt with height. By 30°S, a second upper-

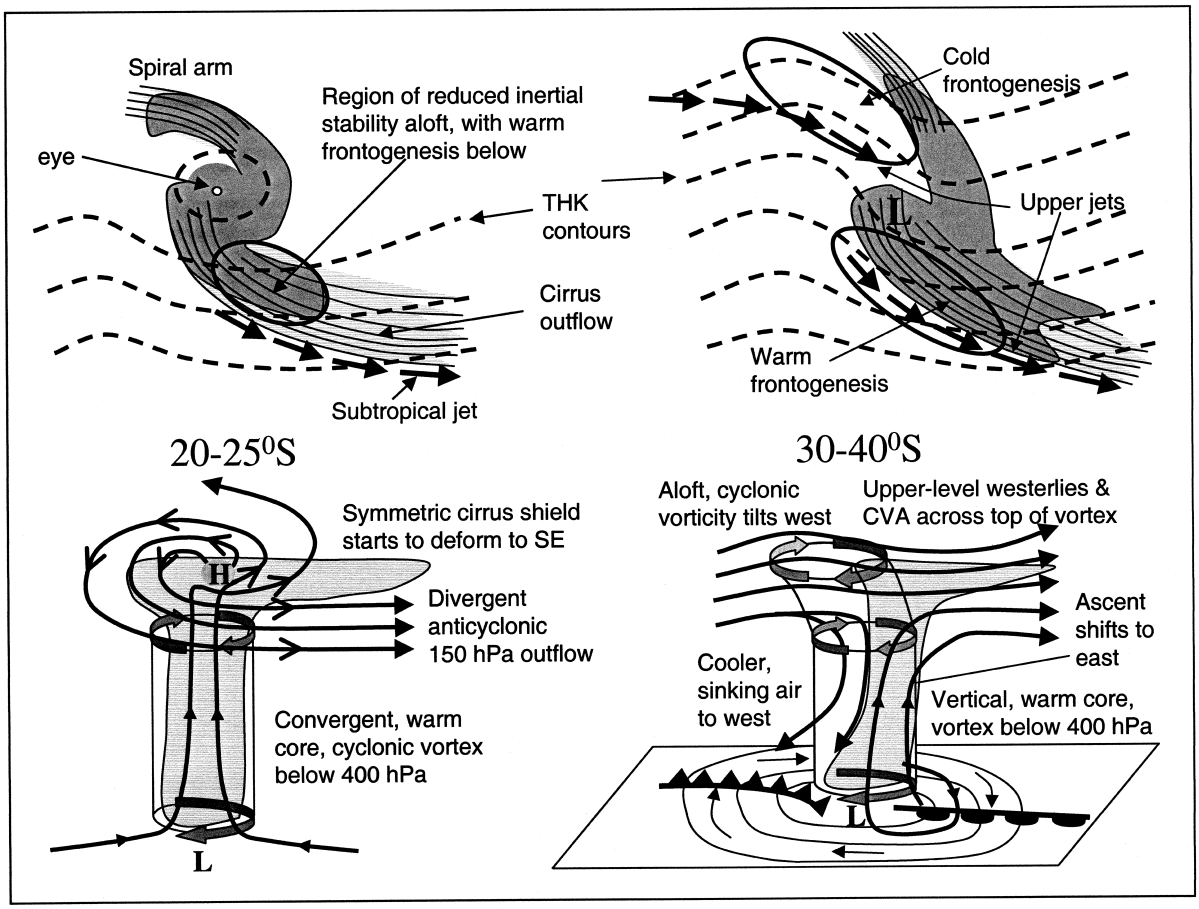

FIG. 15. Conceptual model of extratropical transformation. See text for details.

tropospheric wind maximum and associated region of cold frontogenesis appears west of the storm. Below 400 hPa, the storm retains the vertical, warm convectively unstable cyclonic core.

The unique climatology of the southwest Pacific basin, with westerlies and baroclinity extending to near 15°S raises some interesting questions. On the one hand, strengthening shear is what eventually rips the storm apart by destroying the distinctive storm symmetry and allowing cooler and drier air to invade the western sector. On the other hand, baroclinic effects appear to help the storm under certain circumstances through strengthening the synergy between the outflow layer and the downstream jet. Baroclinic effects can also lead to extratropical reintensification. Numerical modeling of the interaction between a mature hurricane and migratory troughs in the midlatitude westerlies could help determine the precise sequence of events, as in Ritchie and Elsberry (2001). It is clear that the outcome is highly dependent on the nature of the preexisting disturbance in the westerlies, the geometry of the interaction, and the magnitude of the vertical shear, implying that the problem of extratropical regeneration is a multibody problem. As sample sizes from observational data are somewhat limited, numerical modeling might identify more completely the range of possibilities by which these antecedent disturbances become configured and the outcomes that result. This work would lead naturally to the formulation of forecasting rules.

One outstanding issue is a working definition for ET, which is desirable as a basis for forecasting and archiving cases of ET and ensuring meaningful quantitative comparison between ocean basins. In the literature, ET has come to be viewed as a progressive process involving extratropical transformation and possible reintensification. Efforts to define ET must discriminate between ET and TC decay via shearing effects. Clearly, there is a question of how far into the midlatitudes a TC must advance in order to be classed as ET. This study has shown that most southwest Pacific TCs have baroclinic characteristics by 25°S whereas in the NH, the symmetric hurricane structure is commonly preserved poleward of 40°N. Clearly, any geographic component of a taxonomy must differ from basin to basin. There is also subjectivity and uncertainty in assessing whether extratropical transformation has occurred.

TABLE 4. List of southwest Pacific tropical cyclones during 1980–97 progressing poleward of 35°S.

Name	Start date	Start location	End date	End location
Paul	7 Jan 80	21.5°S, 149.0°E	12 Jan 80	47.0°S, 161.0°E
Simon	22 Feb 80	24.7°S, 153.5°E	27 Feb 80	37.0°S, 175.0°W
Sina	10 Mar 80	15.5°S, 159.0°E	16 Mar 80	50.0°S, 173.0°W
Freda	26 Feb 81	15.5°S, 144.6°E	9 Mar 81	35.0°S, 169.8°E
Gyan	18 Dec 81	9.0°S, 172.0°E	29 Dec 81	41.0°S, 166.3°E
Hettie	24 Jan 82	18.2°S, 166.1°E	6 Feb 82	40.0°S, 156.0°W
Bernie	1 Apr 82	5.0°S, 158.3°E	14 Apr 82	40.0°S, 167.5°W
Monica	25 Dec 84	12.8°S, 147.0°E	2 Jan 85	50.0°S, 167.0°E
Hina	11 Mar 85	16.5°S, 174.7°E	20 Mar 85	38.0°S, 155.0°W
Patsy	13 Dec 86	10.4°S, 172.7°E	22 Dec 86	44.5°S, 177.7°E
Bola	24 Feb 88	12.0°S, 180.0°E	11 Mar 88	41.8°S, 170.8°E
Dovi	8 Apr 88	15.0°S, 170.9°E	18 Apr 88	44.3°S, 162.6°W
Eseta	17 Dec 88	14.3°S, 166.3°E	28 Dec 88	36.3°S, 170.5°E
Delilah	30 Dec 88	17.3°S, 150.1°E	7 Jan 89	37.1°S, 168.3°E
Harry	8 Feb 89	17.2°S, 160.9°E	23 Feb 89	49.0°S, 175.9°E
Nancy	28 Jan 90	18.0°S, 156.0°E	8 Feb 90	40.0°S, 170.9°E
Hilda	4 Mar 90	18.5°S, 155.0°E	6 Mar 90	40.9°S, 165.1°E
Daman	15 Feb 92	12.6°S, 170.0°E	23 Feb 92	51.0°S, 158.0°W
Esau	25 Feb 92	15.4°S, 168.5°E	9 Mar 92	37.5°S, 179.0°W
Fran	5 Mar 92	13.0°S, 174.7°W	21 Mar 92	35.5°S, 166.0°W
Mick	5 Feb 93	16.5°S, 173.0°W	11 Feb 93	36.0°S, 179.0°E
Oli	15 Feb 93	15.2°S, 172.8°E	20 Feb 93	35.0°S, 175.1°W
Polly	25 Feb 93	16.0°S, 158.0°E	9 Mar 93	42.5°S, 169.0°W
Rewa	28 Dec 93	9.5°S, 166.5°E	23 Jan 94	40.6°S, 168.3°E
Sarah	19 Jan 94	17.0°S, 170.5°E	4 Feb 94	52.0°S, 157.5°W
Usha	24 Mar 94	11.5°S, 157.5°E	4 Apr 94	47.0°S, 172.0°W
Atu	11 Mar 96	21.0°S, 168.0°E	18 Mar 96	49.0°S, 171.5°W
Beti	21 Mar 96	12.5°S, 170.9°E	2 Apr 96	48.5°S, 175.2°W
Fergus	24 Dec 96	13.1°S, 159.6°E	1 Jan 97	52.0°S, 151.0°W
Drena	3 Jan 97	13.6°S, 167.7°E	13 Jan 97	53.0°S, 174.0°W
Freda	24 Jan 97	20.0°S, 170.0°E	5 Feb 97	53.5°S, 169.5°W
Nameless	23 Feb 97	18.0°S, 159.2°W	2 Mar 97	48.5°S, 164.5°W
Gavin	3 Mar 97	8.8°S, 171.5°E	14 Mar 97	48.0°S, 168.0°W

There is no agreed standard of how much asymmetry or shear a storm must attain in order to be classed as having completed extratropical transformation. Even if there were a standard, results from different analysis products at different resolutions would differ.

This study has examined the climatology of ET and described average structure changes accompanying ET. Unfortunately, the compositing technique smears different ET characteristics associated with differing midlatitude wave types. A second companion paper will examine the important issue of ET variability over the southwest Pacific. This study will address differences between storms that weaken and storms that regenerate during ET, and will assess how the character of the midlatitude circulation affects the subsequent storm evolution. For example, Thorncroft and Jones (2000) and Browning et al. (1998) note that ET characteristics differ for cyclonic versus anticyclonic sheared waves, while Harr et al. (2000) find different characteristics for TCs embedded in confluent versus diffluent background flow. This companion paper will examine whether midlatitude wave patterns over the southwest Pacific fit into one of these NH models and will determine the implications for the structure and evolution of ET.

Acknowledgments. The southwest Pacific tropical cyclone database was kindly provided to NIWA by MetService (formerly New Zealand Meteorological Service) while gridded atmospheric analyses were provided by NCEP. The author is grateful to Cliff Revell for helpful comments on an earlier draft of this manuscript, to Erick Brenstrum of MetService for suggesting the analysis of Fig. 7b and to other MetService forecasters for valuable feedback during a workshop presentation of this work. Two anonymous reviewers provided comments that improved the manuscript. This research was funded by the New Zealand Foundation for Research, Science and Technology under Contract CO1831.

REFERENCES

Basher, R. E., and X. Zheng, 1995: Tropical cyclones in the southwest Pacific: Spatial patterns and relationships to Southern Oscillation and sea surface temperature. *J. Climate*, **8,** 1249–1260.

Bosart, L. F., and D. B. Dean, 1991: The Agnes rainstorm of June 1972: Surface feature evolution culminating in inland storm redevelopment. *Wea. Forecasting*, **6,** 515–537.

Brand, S., and C. P. Guard, 1978: Extratropical storm evolution from tropical cyclones in the western North Pacific Ocean. Tech. Rep. TR 78 02, Naval Environmental Prediction Research Facility, 20 pp.

Brenstrum, E., 1997: The ghost of cyclones past: Drena, Fergus and the Cyclone of '36. *N.Z. Geogr.*, **33**.

Browning, K. A., G. Vaughan, and P. Panagi, 1998: Analysis of an extratropical cyclone after its reintensification as a warm core

extratropical cyclone. *Quart. J. Roy. Meteor. Soc.,* **124,** 2329–2356.
Carr, F. H., and L. F. Bosart, 1978: A diagnostic evaluation of rainfall predictability for Tropical Storm Agnes, June 1972. *Mon. Wea. Rev.,* **106,** 363–374.
DiMego, G. J., and L. F. Bosart, 1982a: The transformation of Tropical Storm Agnes into an extratropical cyclone. Part I: The observed fields and vertical motion computations. *Mon. Wea. Rev.,* **110,** 385–411.
——, and ——, 1982b: The transformation of Tropical Storm Agnes into an extratropical cyclone. Part II: Moisture, vorticity and kinetic energy budgets. *Mon. Wea. Rev.,* **110,** 412–433.
Dvorak, V. F., 1975: Tropical cyclone intensity analysis and forecasting from satellite imagery. *Mon. Wea. Rev.,* **103,** 420–430.
——, 1984: Tropical cyclone intensity analysis using satellite data. NOAA Tech. Rep. NESDIS 11, U.S. Dept. of Commerce, Washington, DC, 47 pp.
Elsberry, R. L., W. M. Frank, G. J. Holland, J. D. Jarrell, and R. L. Southern, 1987: A global view of tropical cyclones. Dept. of Meteorology, Naval Postgraduate School, Monterey, CA, 185 pp.
Foley, G. R., and B. N. Hanstrum, 1994: The capture of tropical cyclones by cold fronts off the west coast of Australia. *Wea. Forecasting,* **9,** 577–592.
Frank, W. M., and E. A. Ritchie, 1999: Effects of environmental flow upon tropical cyclone structure. *Mon. Wea. Rev.,* **127,** 2044–2061.
Harr, P. A., and R. L. Elsberry, 2000: Extratropical transition of tropical cyclones over the western North Pacific. Part I: Evolution of structural characteristics during the transition process. *Mon. Wea. Rev.,* **128,** 2613–2633.
——, R. L. Elsberry, and T. F. Hogan, 2000: Extratropical transition of tropical cyclones over the western North Pacific. Part II: The impact of midlatitude circulation characteristics. *Mon. Wea. Rev.,* **128,** 2634–2653.
Hart, R. E., and J. L. Evans, 2001: A climatology of the extratropical transition of Atlantic tropical cyclones. *J. Climate,* **14,** 546–564.
Hastings, P. A., 1990: Southern Oscillation influences on tropical cyclone activity in the Australian/South-west Pacific region. *Int. J. Climatol.,* **10,** 291–298.
Hill, H. W., 1970: The precipitation in New Zealand associated with the cyclone of early April 1968. *N.Z. J. Sci.,* **13,** 641–662.
Holland, G. J., 1983: Tropical cyclones in the Australian/southwest Pacific region. Dept. of Atmospheric Science, Paper 363, Colorado State University, Fort Collins, CO, 264 pp.
——, and R. T. Merrill, 1984: On the dynamics of tropical cyclone structural changes. *Quart. J. Roy. Meteor. Soc.,* **110,** 723–745.
Jones, S. C., 1995: The evolution of vortices in vertical shear. I: Initially barotropic vortices. *Quart. J. Roy. Meteor. Soc.,* **121,** 821–851.
Kalnay, E., and Coauthors, 1996: The NCEP/NCAR 40-Year Reanalysis Project. *Bull. Amer. Meteor. Soc.,* **77,** 437–471.
Kerr, I. S., 1976: Tropical storms and hurricanes in the southwest Pacific. New Zealand Meteorological Service Misc. Pub. 148, 114 pp.
Kistler, R., and Coauthors, 2001: The NCEP–NCAR 50-Year Reanalysis: Monthly means CD-ROM and documentation. *Bull. Amer. Meteor. Soc.,* **82,** 247–267.
Klein, P. M., P. A. Harr, and R. L. Elsberry, 2000: Extratropical transition of western North Pacific tropical cyclones: An overview and conceptual model of the transformation stage. *Wea. Forecasting,* **15,** 373–395.
Littlejohn, R. N., 1984: Extreme winds and forest devastation resulting from cyclone ''Bernie.'' *Wea. Climate,* **4,** 47–52.
Malmquist, D., 1999: Meteorologists and insurers explore extratropical transition of tropical cyclones. *Eos, Trans. Amer. Geophys. Union,* **80,** 79–80.
Muramatsu, T., 1985: A study on the changes of the three-dimensional structure and movement speed of the typhoon through its life time. Tech. Rep. 14, Meteorological Research Institute (Japan), 117 pp.
Nichols, N., 1984: The Southern Oscillation, sea-surface temperature, and interannual fluctuations in Australian tropical cyclone activity. *J. Climatol.,* **4,** 661–670.
Palmén, E., 1958: Vertical circulation and release of kinetic energy during the development of Hurricane Hazel into an extratropical storm. *Tellus,* **10,** 1–21.
Petterssen, S., 1936: Contribution to the theory of frontogenesis. *Geofys. Publ.,* **11** (6), 1–27.
Radford, D., R. Blong, A. M. d'Aubert, I. Kuhnel, and P. Nunn, 1996: Occurrence of tropical cyclones in the southwest Pacific region. Greenpeace Report, 35 pp. [Available from Greenpeace International, Keizersgracht 176, 1016 DW Amsterdam, Netherlands.]
Revell, C. G., 1981: Tropical cyclones in the southwest Pacific, Nov. 1969 to April 1979. New Zealand Meteorological Service Misc. Pub. 170, 53 pp.
——, 1985: Tropical Cyclone Saba. *Wea. Climate,* **5,** 42–51.
——, 1986: Tropical Cyclone Namu. *Wea. Climate,* **6,** 67–69.
——, 1987: The 1986/87 hurricane season in the South Pacific. *Wea. Climate,* **7,** 38–54.
——, and S. W. Goulter, 1986a: South Pacific tropical cyclones and the Southern Oscillation. *Mon. Wea. Rev.,* **114,** 1138–1145.
——, and ——, 1986b: Lagged relations between the Southern Oscillation and numbers of tropical cyclones in the South Pacific region. *Mon. Wea. Rev.,* **114,** 2669–2670.
Reynolds, R. W., 1988: A real-time global sea surface temperature analysis. *J. Climate,* **1,** 75–86.
Ritchie, E. A., and R. L. Elsberry, 2001: Simulations of the transformation stage of the extratropical transition of tropical cyclones. *Mon. Wea. Rev.,* **129,** 1462–1480.
Sawyer, J. S., 1950: Formation of secondary depressions in relation to the thickness pattern. *Meteor. Mag.,* **79,** 1–5.
Schultz, D. M., D. Keyser, and L. F. Bosart, 1998: The effect of large-scale flow on low-level frontal structure and evolution in midlatitude cyclones. *Mon. Wea. Rev.,* **126,** 1767–1791.
Shapiro, M. A., and D. Keyser, 1990: Fronts, jets streams and the tropopause. *Extratropical Cyclones—The Erik Palmén Memorial Volume,* C. W. Newton and E. O. Holopainen, Eds., Amer. Meteor. Soc., 167–191.
Sinclair, M. R., 1993a: Synoptic-scale diagnosis of the extratropical transition of a southwest Pacific extratropical cyclone. *Mon. Wea. Rev.,* **121,** 941–960.
——, 1993b: A diagnostic study of the extratropical precipitation resulting from tropical cyclone Bola. *Mon. Wea. Rev.,* **121,** 2690–2707.
——, 1997: Objective identification of cyclones and their circulation intensity, and climatology. *Wea. Forecasting,* **12,** 591–608.
——, and X. Cong, 1992: Polar airstream cyclogenesis in the Australasian region: A composite study using ECMWF analysis. *Mon. Wea. Rev.,* **120,** 1950–1972.
——, and M. Revell, 2000: Classification and composite diagnosis of extratropical cyclogenesis events in the southwest Pacific. *Mon. Wea. Rev.,* **128,** 1089–1105.
Thompson, C. S., S. Ready, and X. Zheng, 1992: Tropical cyclones in the southwest Pacific: November 1979 to May 1989. New Zealand Meteorological Service, 35 pp.
Thorncroft, C., and S. C. Jones, 2000: The extratropical transitions of Hurricanes Felix and Iris in 1995. *Mon. Wea. Rev.,* **128,** 947–972.
Tomlinson, A. I., 1975: Cyclone Alison. New Zealand Meteorological Service Tech. Information Circular 148, 26 pp.
Trenberth, K. E., 1977: A diagnostic investigation of the behaviour of tropical cyclone Norman. New Zealand Meteorological Service Tech. Note 231, 26 pp.
Uccellini, L. W., and P. C. Kocin, 1987: The interaction of jet streak circulations during heavy snow events along the east coast of the United States. *Wea. Forecasting,* **2,** 289–308.